This is not the published version of the article / Þetta er ekki útgefna útgáfa greinarinnar

Author(s)/Höf.:	Kleine Barbara I. Kleine, Andri Stefánsson, Ríkey Kjartansdóttir, Simon Prause, Tobias B. Weisenberger, Hannah I.Reynolds, Árný E. Sveinbjörnsdóttir, Marie D. Jackson, Magnús T. Gudmundsson
Title/Titill:	The Surtsey volcano geothermal system: An analogue for seawater-oceanic crust interaction with implications for the elemental budget of the oceanic crust
Year/Útgáfuár:	2020
Version/Útgáfa:	Pre-print (óritrýnt handrit)

Please cite the original version:

Vinsamlega vísið til útgefnu greinarinnar:

Kleine, B. I., Stefánsson, A., Kjartansdóttir, R., Prause, S., Weisenberger, T. B., Reynolds, H. I., . . . Gudmundsson, M. T. (2020). The Surtsey volcano geothermal system: An analogue for seawater-oceanic crust interaction with implications for the elemental budget of the oceanic crust. *Chemical Geology, 550*, 119702. Doi:https://doi.org/10.1016/j.chemgeo.2020.119702

The Surtsey volcano geothermal system: an analogue for seawater-oceanic crust

interaction with implications for the elemental budget of the oceanic crust

Barbara I. Kleine[1]*, Andri Stefánsson[1], Ríkey Kjartansdóttir[1], Simon Prause[2,3], Tobias B. Weisenberger[3], Hannah I. Reynolds[1], Árný E. Sveinbjörnsdóttir[1], Marie D. Jackson[4], Magnús T. Gudmundsson[1]

[1]Institute of Earth Sciences, University of Iceland, Reykjavík, Iceland

[2]School of Engineering and Natural Sciences, University of Iceland, Reykjavík, Iceland

[3]Iceland GeoSurvey, Reykjavík, Iceland

[4]Department of Geology and Geophysics, University of Utah, Salt Lake City, USA

*corresponding author: barbarak@hi.is

Abstract

Surtsey is a young volcanic island in the offshore extension of Iceland's southeast rift zone that grew from the seafloor during explosive and effusive eruptions in 1963-1967. In 1979, a cored borehole (SE-1) was drilled to 181 m depth and in 2017 three cored boreholes (SE-2a, SE-2b and SE-3) were drilled to successively greater depths. The basaltic deposits host a low-temperature (40-141 °C) seawater-dominated geothermal system. Surtsey provides an ideal environment to study water-rock interaction processes in a young seawater geothermal system. Elemental concentrations (SiO_2, B, Na, Ca, Mg, F, dissolved inorganic carbon, SO_4, Cl) and isotope contents (δD, $\delta^{18}O$) in borehole fluids indicate that associated geothermal waters in submarine deposits originated from seawater modified by reactions with the surrounding basalt. These processes produce authigenic minerals in the basaltic lapilli tuff and a corresponding depletion of certain elements in the residual waters. Coupling of measured and modeled concentrations investigates the effect of temperature and associated abundance of authigenic minerals on chemical fluxes from and to the igneous oceanic crust during low-temperature alteration. The annual chemical fluxes calculated at 50-150 °C range from -0.01 to $+0.1×10^{12}$ mol yr^{-1} for SiO_2, +0.2 to $+129×10^{12}$ mol yr^{-1} for Ca, -129 to $-0.8×10^{12}$ mol yr^{-1} for Mg and -21 to $+0.4×10^{12}$ mol yr^{-1} for SO_4 where negative values indicate chemical fluxes from the ocean into the oceanic crust and positive values indicate fluxes from the oceanic crust to the oceans. These flux calculations reveal that water-rock interaction at varying water-rock ratios and temperatures produces authigenic minerals that serve as important sinks of seawater-derived SiO_2, Mg and SO_4. In contrast, water-rock interaction accompanied by dissolution of

33 basaltic glass and primary crystal fragments, provides a significant source of Ca. Such low-

34 temperature alteration could effectively influence the elemental budget of the oceanic igneous

35 crust and ocean waters. The modelling provides insights into water chemistries and chemical

36 fluxes in low-temperature MOR recharge zones. Surtsey also provides a valuable young

37 analogue for assessing the chemical evolution of fluid discharge over the life cycles of

38 seamounts in ridge flank systems.

39

40 **Keywords**

41 Surtsey volcano, water-rock interaction, elemental mobility, oceanic crust, ICDP, SUSTAIN

42

43 **1. Introduction**

44 The advective heat loss from the oceanic crust is greater at mid-ocean ridge (MOR) flanks than

45 at ridge axes (Sclater et al., 1980; Stein and Stein, 1994). The large heat loss in these low-

46 temperature environments occurs through a seawater flux in the oceanic crust of ridge flanks

47 that is significantly larger $(0.2\text{-}5.4\times10^{17}$ kg yr^{-1}) than the seawater flux in ridge axes

48 $(\sim0.72\times10^{13}$ kg yr^{-1}) (Nielsen et al., 2006). Chemical changes accompany the larger fluxes as

49 the infiltrating seawater into the oceanic crust will ultimately interact with the surrounding

50 rocks. Thus, the geochemistry of seawater percolating through geothermal systems within the

51 oceanic crust is largely controlled by processes such as water-rock interaction and phase

52 separation at varying water-rock ratios, temperatures and pressures (Allen and Seyfried Jr,

53 2003; Bowers et al., 1988; Humphris and Klein, 2018; Von Damm, 1995). This may produce

54 chemical fluxes with important effects on oceanic elemental budgets (Alt, 2003; Elderfield and

55 Schultz, 1996; Huang et al., 2018; Mottl and Wheat, 1994; Sansone et al., 1998; Staudigel,

56 2014; Wheat et al., 1996; Wheat and Mottl, 2000). These low-temperature geothermal systems

57 may act as important sinks of seawater K, Mg and SO$_4$ and sources of seawater Ca, Sr and SiO$_2$

58 (Wheat and Mottl, 2000). The chemistry of fluids emitted from ridge flank systems differs from

59 vent fluids discharged at mid-ocean ridges (Kadko et al., 1994; Wheat and Mottl, 2000). The

60 flank system fluids have higher concentrations of Mg, Sr, SO$_4$ and SiO$_2$, whereas the

61 concentrations of K, Ca, B and Fe are similar or lower than those measured in vent fluids.

62 These differences highlight the importance of new investigations of other low-temperature

63 aquifers, such as MOR recharge zones and their contribution to global elemental cycling in the

64 oceanic crust. Moreover, the geochemistry of the fluids circulating through the igneous crust

65 may be obscured by interactions with overlying sediments as they upwell to the seafloor (Alt,

66 2003; James et al., 2003). Thus, chemical flux estimates for Ca, SiO$_2$, Mg and SO$_4$ may not be

67 representative of true chemical fluxes for the igneous oceanic crust in ridge flank systems. This
68 discrepancy may lead to uncertainties in calculations of the global elemental flux to the oceans.

69   Iceland exhibits the only MOR on Earth that exposes a largely submarine rift on land.
70 Thus, seawater dominated geothermal systems in Iceland, such as Reykjanes and Svartsengi,
71 serve as valuable analogues for hydrothermal vent systems on the seafloor, in terms of
72 authigenic mineralization, geothermal solutions and primary lithologies (Hannington et al.,
73 2005; Hardardóttir et al., 2009; Hardardóttir et al., 2013; Kadko et al., 2007; Kleine et al., 2020;
74 Kleine et al., 2018; Marks et al., 2011; Marks et al., 2015; Michard et al., 1984; Mottl and
75 Holland, 1978). Surtsey volcano is located in the southern offshore extension of the Icelandic
76 eastern rift zone (Einarsson, 2008; Jakobsson et al., 2009; Thorarinsson et al., 1964) (Fig. 1).
77 It provides a unique environment for studying geothermal processes and seawater-rock
78 interactions in low-temperature vent systems of the oceanic crust, in the range of 50-150 °C.
79 The subsurface of the island was first explored through a 181 m cored borehole drilled in 1979,
80 12 years after eruptions terminated (Jakobsson and Moore, 1982, 1986; Jakobsson et al., 2009).
81 Three new cored boreholes were drilled in 2017 by the Surtsey Underwater volcanic System
82 for Thermophiles, Alteration processes and INnovative concretes (SUSTAIN) drilling project,
83 funded in part by the International Continental Scientific Drilling Program (ICDP) (Jackson et
84 al., 2019b; Weisenberger et al., 2019).

85   The effects of seawater-rock interaction on the chemical compositions of water samples
86 retrieved in 2016-2018 from the basaltic subsurface deposits from the 1979 borehole, SE-1,
87 and an inclined 2017 borehole, SE-3, are investigated by this study (Fig. 1). Measured
88 concentrations of SiO_2, B, Na, Ca, Mg, F, dissolved inorganic carbon (DIC), SO_4 and Cl in the
89 borehole waters acquired through downhole sampling using a bailer sampler are described.
90 These descriptions provide a context for evaluating chemical changes in the 50-year-old
91 Surtsey system within low-temperature MOR recharge zones. Elemental fluxes for SiO_2, Ca,
92 Mg and SO_4 are constrained using a geochemical reaction path modeling approach. The
93 modeling results for the geochemistry of Surtsey waters are then compared with available data
94 from relevant ridge flank and seamount systems. They provide further insights on the
95 significance of MOR-related low-temperature hydrothermal systems on the global elemental
96 budget of the oceanic crust.

97
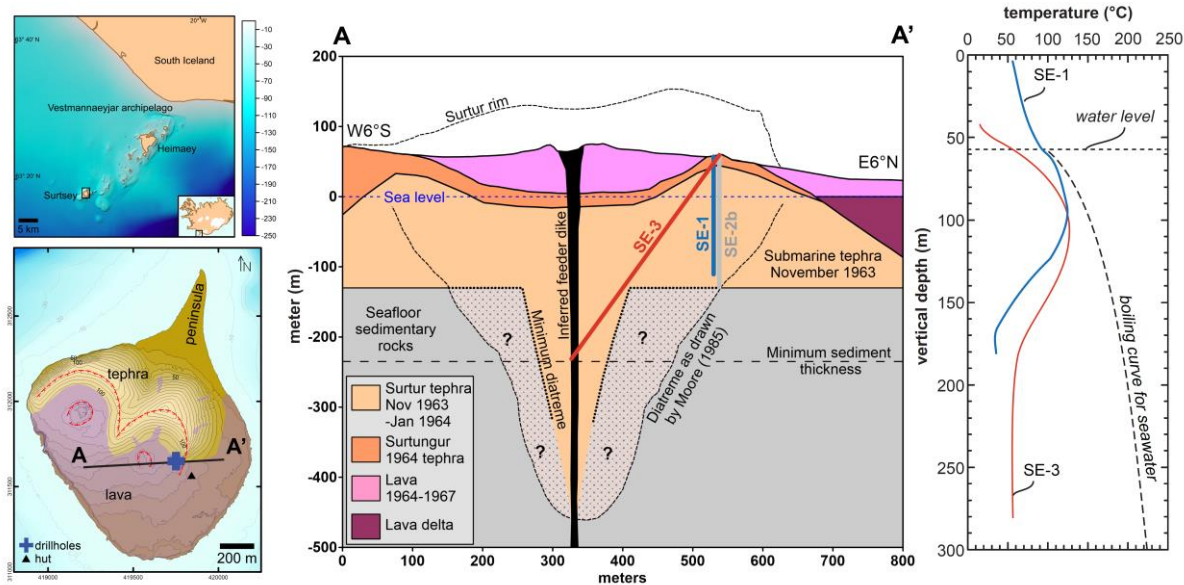
Figure 1. Location of the 1979 borehole, SE-1, and the 2017 boreholes, SE-2b and SE-3, and corresponding temperature profiles measured in 2017. The Surtsey subsurface observatory occupies the SE-2b borehole (Türke et al., 2019). Water samples were collected from SE-1 in 2016 and 2017 and from SE-3 in 2018. Maps and the schematic cross section of Surtsey are modified from Jackson et al. (2019b).

2. The geothermal system at Surtsey and the ICDP SUSTAIN project

The island of Surtsey forms the southernmost extension of the Vestmannaeyjar volcanic system off the south coast of Iceland (Fig. 1). The island was created by explosive and effusive basaltic eruptions from 1963 to 1967; it grew from a seafloor depth of ~130 m below sea level to a height of 150 m above sea level (Jakobsson et al., 2009; Thorarinsson et al., 1964; Thors and Jakousson, 1982). The approximately 1 km^3 of eruptive products include basaltic tuff, tephra, and lava flows (Schipper et al., 2015; Thorarinsson et al., 1964). Basaltic intrusions and lithified deposits of basaltic tuff and tephra host a geothermal system (Jakobsson and Moore, 1986). Thermal anomalies were first observed on the surface of Surtsey in spring 1967 (Friedman and Williams, 1970). The thermal area expanded through 1979; thereafter, tephra consolidation to form lithified tuff may have influenced the heat flux through the surface deposits. Temperatures measured in 1980 within the submarine sections of the cased SE-1 borehole ranged from ~40 °C at 180.3 m to 141 °C at 100-108 m measured depth. Rapid alteration and consolidation of the basaltic tephra occurred through palagonitization processes (Jakobsson, 1978), which produced authigenic clay minerals, zeolite, tobermorite, anhydrite, and calcite (Jakobsson and Moore, 1986). The heat in the hydrothermal system was thought to

4

120 have been provided by basaltic intrusions into the freshly erupted tephra (Jakobsson et al.,
121 2000; Jakobsson and Moore, 1982, 1986; Stefánsson et al., 1985).

122   The continuously cored SE-1 borehole drilled in 1979 (Jakobsson and Moore, 1982) is
123 thought to terminate a few meters above the pre-eruption sea floor (Fig. 1). Investigations of
124 the 1979 drill core have provided numerous insights into the structure of the island and the
125 rapid geothermal alteration of the tephra (Jakobsson and Moore, 1982, 1986). The three 2017
126 cored boreholes acquired through the ICDP SUSTAIN drilling project (Jackson et al., 2019b;
127 Weisenberger et al., 2019) include two vertical cores (SE-2a and SE-2b) drilled parallel to the
128 SE-1 core to 152 and 192 m depth below the ground surface. An inclined borehole (SE-3) with
129 a plunge of 55° and azimuth of 264° extended to a measured depth of 354 m beneath Surtur
130 crater (Fig. 1), terminating about 100 m below the pre-eruption seafloor. Seawater was used as
131 drilling fluid. All the boreholes traversed basaltic tuff (or tephra) and none traversed deposits
132 of the pre-eruption seafloor (Jackson et al., 2019b).

133   Temperatures were recorded in the SE-1 borehole on August 8, 2017 before the
134 initiation of SUSTAIN drilling. Temperatures were recorded in the cased SE-3 borehole on
135 September 9, 2017, six days after drilling terminated (Jackson et al., 2019b) (Fig 1). Cooling
136 could have occurred from seawater circulating fluid during drilling, yet temperature
137 measurements of borehole waters obtained from SE-3 in summer 2018 gave similar results
138 (Table 1). The temperature anomaly at about 100 m vertical depth in the SE-1 borehole has a
139 similar form in the SE-3 borehole. No substantial sections of intrusive basalt were traversed in
140 the 2017 drilling and, therefore, the hypothesis of Jakobsson and Moore (1986) has been
141 partially revised to include the possibility of a broad zone of heat transfer into the upper
142 submarine deposits from the thick lava shield that formed from 1964 to 1967 in Surtur crater
143 (Moore and Jackson, in press). Geophysical logging of the SE-02b borehole on August 26,
144 2017, recorded deviations in temperature, fluid and rock resistivity, the vertical pressure
145 gradient and derived salinity in a zone between 143-150 m measured depth (Jackson et al.,
146 2019b). This zone correlates with porous layers in the 1979 borehole that were thought to
147 channel cool seawater into the geothermal system (Jakobsson and Moore, 1982, 1986; Ólafsson
148 and Riley, 1978). Low temperatures in the loosely-consolidated tephra of the SE-1 borehole
149 may therefore record this zone of seawater inflow as well as the proximity to the cool
150 sedimentary rock of the pre-eruption seafloor. The low temperatures in the deep sub-seafloor
151 basaltic lapilli tuff of borehole SE-3 persisted in 2018 borehole temperature measurements.
152 They indicate that the basaltic deposits of a postulated diatreme (Jackson et al., 2019b; Moore,

153 1985; Moore and Jackson, in press) are not yet in thermal equilibrium with the cool seafloor
154 sedimentary host rock.

155 In this study, water samples were collected along depth profiles from the SE-1 and SE-
156 3 boreholes with the purpose of studying chemical variations in the acquired fluids. Both
157 boreholes are fully cased with stainless steel drill pipes emplaced during drilling (Weisenberger
158 et al., 2019). Inflow of geothermal water into the cased boreholes may occur through tephra
159 and tuff deposits at their lowermost depths (Jackson et al., 2019b; Jakobsson and Moore, 1982).
160 A subsurface observatory occupies borehole SE-2b (Türke et al., 2019), so it was not available
161 for water extractions during the sampling periods. Borehole SE-2a collapsed during the drilling
162 operations (Jackson et al., 2019b; Weisenberger et al., 2019).

163

164 **3. Methods**

165 *3.1. Water sampling*

166 Water samples from variable depths in borehole SE-1 were collected on 6 September 2016 and
167 on 5 September 2017, at the termination of SUSTAIN drilling. The purpose of taking water
168 samples in the cased boreholes at depth intervals was to evaluate potential in-borehole
169 processes that could interfere with the chemical and isotopic composition of waters in the
170 boreholes that could be representative for water-rock interaction processes in the surrounding
171 host rocks. The water in the cased boreholes is considered to be connected to the groundwater
172 system of the island because the tidal range can be measured within the holes (Jackson et al.,
173 2019b; Weisenberger et al., 2019). The lowermost samples obtained from each borehole are
174 presumed to be most representative of the deep circulating fluids interacting with the host rocks
175 at Surtsey. They are located either just below the open base of the casing of SE-1 or just above
176 it in SE-3 and thus indicate samples that are likely to be in direct contact with the host rocks.

177 Water samples in borehole SE-3 were collected on 20 July 2018, 10 months after the
178 termination of SUSTAIN drilling (Table 1). In all sampling sessions, a stainless-steel bailer
179 attached to a slickline was lowered to the sampling depth (Fig. 2). The bailer was equipped
180 with a glass-fiber jar that could move freely along the slickline. At the sampling depth the jar
181 was sent down the wire to mechanically close the bailer, at which point both were pulled up to
182 surface. The maximum volume of water retrieved was 1.5 L per sampling depth. Water samples
183 for pH, dissolved inorganic carbon (DIC), and stable water isotope (δD and δ^{18}O)
184 measurements were collected in gas tight 50-250 mL amber glass bottles. Water samples for
185 major cation analyses were filtered through a 0.2 μm filter (cellulose acetate) into
186 polypropylene bottles and acidified to 1% by addition of HNO$_3$ (Suprapur® Merck) on site.

187   Water samples for anion determination were also filtered through a 0.2 µm filter (cellulose

188   acetate) into polypropylene bottles on site, but not further treated.

189

190   *3.2. Core sampling*

191   Sampling of the 2017 drill core was carried out on site during the ICDP SUSTAIN drilling

192   operation (Weisenberger et al., 2019). Drill cores were collected in 3 m lengths of plastic core

193   liners and stored in these liners at the drill site before transport off island. A ~10 cm length of

194   core was cut from the upper part of the third 1 m core section of the complete core run. The

195   samples were thus acquired at 9-10 m increments through each borehole. To minimize

196   alteration or further contamination, the 10 cm core lengths were kept inside the plastic liner,

197   sealed air-tight into plastic bags and stored at 4 °C on site until sample preparation in the

198   laboratory.

199

200   *3.3 Chemical analyses*

201   The pH of the water samples was analyzed at 21 °C using a pH meter and electrode

202   calibrated with commercial buffer solutions. The analytical precision was ±0.1. Measurements

203   of DIC concentrations used a modified alkalinity titration (Stefánsson et al., 2007). Major

204   elemental analyses (SiO_2, Cl, Na, K, Al, Fe, Mg, SO_4, Ca, B) were carried out using ICP-OES

205   (Spectro Ciros Vision). Concentrations of F were measured with a fluorine ion-selective

206   electrode. The analytical precision of major element and F analyses was based on duplicate

207   analysis of the samples and found to be in all cases <5% at the 95% confidence level. A

208   correction factor was applied to the measured F concentrations to account for the formation of

209   MgF^+ complexes (see Appendix A for details).The stable isotope analysis of water (δD and

210    $\delta^{18}O$) was conducted using a Thermo Delta V advantage isotope ratio mass spectrometer

211   (IRMS). Results are reported relative to Vienna Standard Mean Ocean water (VSMOW). The

212   analytical precision obtained by repeated analysis of the samples was <1.0‰ for δD and <0.1‰

213   for $\delta^{18}O$.

214   Representative rock samples were selected to study the alteration mineralogy of the

215   1979 and 2017 drill cores. For this study, polished thin sections were produced for core

216   segments at measured depths of 20 and 90 m in borehole SE-1 and 280 m in borehole SE-3.

217   These thin sections include the principal authigenic mineral phases identified by Jakobsson and

218   Moore (1986). The chemical compositions of these minerals were studied and analyzed with a

219   HITACHI TM-3000 scanning electron microscope (SEM) with an accelerating voltage of 15

220   keV and a JEOL JXA-8230 electron microprobe (EMP) analyzer equipped with a LaB6

electron emitter at the Institute of Earth Sciences at University of Iceland. Running conditions for EMP analyses were 15 keV accelerating voltage and 10 nA cup current with a beam diameter of 1 to 10 µm.
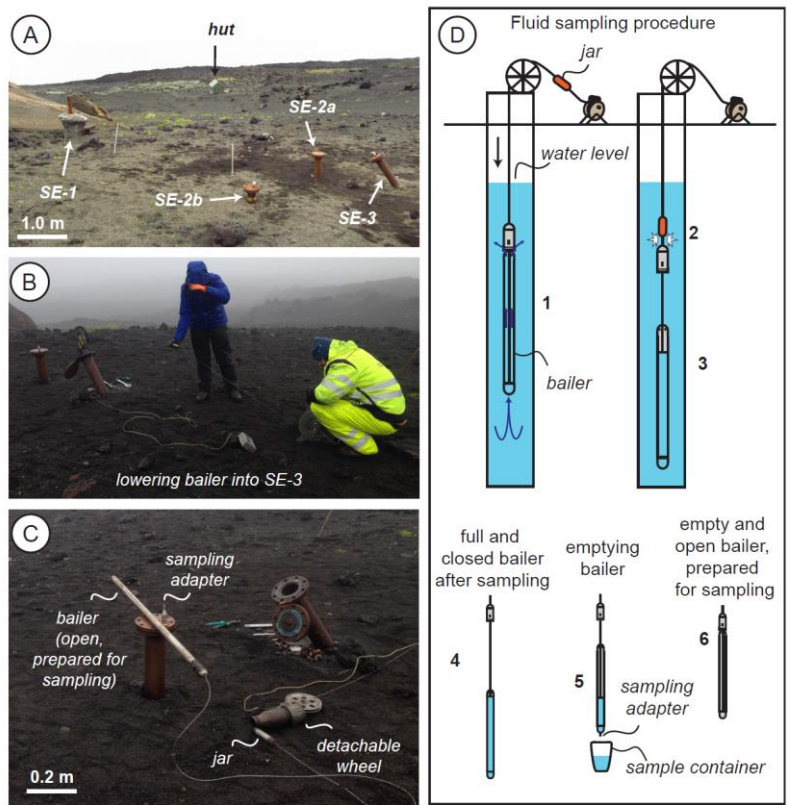
Figure 2. *Water sampling from boreholes SE-1 and SE-3 at Surtsey in summer 2018 (A-C). (D) Water sampling procedure: (1) the open bailer is lowered into the borehole to the desired sampling depth. Water passes freely through the bailer during the descent, (2) a glass-fiber jar is sent down the wire to mechanically snap shut the bailer at the sampling depth, (3) the sealed bailer is pulled up to the surface, (4) the sampled water is retrieved from the bailer by attaching a sample adapter to the lower end of the bailer, (5) after emptying, the adapter is removed, (6) the bailer is opened and prepared for the retrieval of a subsequent sample.*

3.4. Geochemical modeling

Geochemical modeling was carried out to investigate the potential influences of water-rock interaction and accompanying authigenic mineral formation on water chemistry in low-temperature seawater-dominated geothermal systems. Geochemical calculations, including mineral saturation state and reaction path calculations, were performed with the aid of the PHREEQC program using an updated version of the LLNL (Lawrence Livermore National

239   Library) database (Parkhurst and Appelo, 1999). For these calculations, the measured pH

240   values at room temperature were corrected to the water sampling temperatures measured in the

241   Surtsey boreholes assuming conservation of alkalinity. The thermodynamic database was

242   updated to include modified mineral solubilities for low-temperature authigenic minerals of

243   interest, such as zeolites (Johnson et al., 1982; Neuhoff, 2000), clay minerals (Catalano, 2013;

244   Gysi and Stefánsson, 2011) and calcium-silicate-hydrates (this study; Blanc et al., 2010;

245   Lothenbach et al., 2008; Sarkar et al., 1982). The water-rock interaction modeling included

246   conventional reaction path simulations in which seawater was allowed to react with basaltic

247   glass in steps and in which the stable or saturated authigenic minerals in each step were allowed

248   to precipitate (Gysi and Stefánsson, 2011; Stefánsson, 2010). The chemical compositions of

249   both seawater and basaltic glass used in the modeling calculations are listed in Table 2. The

250   simulations were carried out at 50, 100 and 150°C. The authigenic minerals used in the

251   calculations were those observed in the geothermal system at Surtsey (this study; Jakobsson

252   and Moore, 1986) and other low-temperature geothermal aquifers hosted in the oceanic crust

253   (e.g., Alt et al., 1996). They include calcite, anhydrite, clay minerals, Al-tobermorite and

254   zeolites. Mineral compositions from EMP analyses (Table 3) were considered to constrain their

255   solubilities using a combination of oxide summation techniques (see Appendix A for details).

256   To evaluate the effects of variable redox conditions on the formation of certain authigenic

257   minerals (e.g., clays, carbonates, sulphates), the availability of oxidized and reduced S and Fe

258   species in the reacting solution was varied by allowing the formation of minerals with changing

259    $Fe(II)/Fe(III)$ and $S(-II)/S(VI)$ ratios.

260

261   **4. Results**

262   *4.1. Chemical and isotopic composition of geothermal water*

263   The chemical compositions of the water samples are listed in Table 1. The pH measurements

264   range from mildly acidic to mildly alkaline (5.07-8.01). In borehole SE-1, the elemental

265   concentrations of SiO_2 (0.096-0.374 mmol kg^{-1}), B (0.321-0.383 mmol kg^{-1}), Na (469-514

266   mmol kg^{-1}), K (10.9-11.6 mmol kg^{-1}), Ca (12.6-24.7 mmol kg^{-1}), Mg (17.4-27.8 mmol kg^{-1}),

267   Fe (0.021-0.418 mmol kg^{-1}), Al (0.003-0.074 mmol kg^{-1}), F (0.028-0.040 mmol kg^{-1}), Cl (522-

268   611 mmol kg^{-1}), CO_2 (0.426-2.1 mmol kg^{-1}) and SO_4 (10.8-19.4 mmol kg^{-1}) are more variable,

269   as compared to the corresponding elemental concentrations of water extracted from SE-3 (Fig.

270   3). In SE-3, elemental concentrations of SiO_2 (0.081-0.227 mmol kg^{-1}), Na (462-489 mmol kg^{-1}

271   ^{1}), Ca (9.17-13.1 mmol kg^{-1}), F (0.046-0.073 mmol kg^{-1}) and Cl (540-567 mmol kg^{-1}) are

272   similar to corresponding concentrations measured in seawater (Bruland, 1983). Concentrations

273   of B (0.270-0.358 mmol kg^{-1}), Mg (36.3-39.9 mmol kg^{-1}), CO_2 (0.489-1.03 mmol kg^{-1}) and

274   SO_4 (14.8-21.3 mmol kg^{-1}) are considerably lower than corresponding seawater concentrations,

275   whereas concentrations of K (10.2-10.7 mmol kg^{-1}), Fe (0.016-0.207 mmol kg^{-1}) and Al (0.002-

276   0.045 mmol kg^{-1}) are slightly higher (Fig. 3). A detailed description of possible in-borehole

277   mixing processes affecting water chemistries can be found in Appendix A.

278   The δD and $\delta^{18}O$ values measured in water samples from boreholes SE-1 and SE-3 are

279   reported in Table 1 and shown in Figure 4. The δD (+15.6 to +33.2‰) and $\delta^{18}O$ (+4.0 to

280   +9.6‰) values in borehole SE-1 are significantly more positive than the corresponding

281   measurements in SE-3 ($\delta D = 3.2 \pm 0.6$‰; $\delta^{18}O = +0.4 \pm 0.08$‰) as well as the seawater

282   reference ($\delta D = 0 \pm 5$‰; $\delta^{18}O = 0 \pm 0.5$‰) (Ólafsson and Riley, 1978).

283

4.2. Authigenic mineralogy and chemistry

285 The dominant authigenic minerals observed through petrographic and EMP analyses in the

286 submarine tuff samples acquired from the 1979 and 2017 drill core include calcite, anhydrite,

287 analcime, phillipsite, smectitic clay minerals, as well as Al-tobermorite, an unusual layered

288 calcium-aluminum-silicate-hydrate mineral (Jackson et al., 2013). These are the same

289 authigenic minerals identified by Jakobsson and Moore (1986). Clay minerals appear as

290 alteration products encasing primary volcanic crystal fragments, such as olivine, and in altered

291 glass (Fig. 5). Analcime, anhydrite, calcite and Al-tobermorite occur mainly in pores and

292 vesicles, the altered vitric matrix, and occasional cracks. The representative chemical

293 compositions of these minerals are listed in Table 3. Calcite and anhydrite have almost pure

294 Ca-endmember compositions. Zeolites, such as analcime, contain small amounts of Ca and K.

295 Smectitic clay minerals in altered glass are mainly composed of Fe-Mg saponite with a minor

296 nontronite component. The Al-tobermorite contains ~2.5 wt.% Al and incorporates Na and K

297 cations, similar to crystals with 11 Å interlayer spacing in diverse geologic environments

298 (Jackson et al., 2017; Jakobsson and Moore, 1986).

299
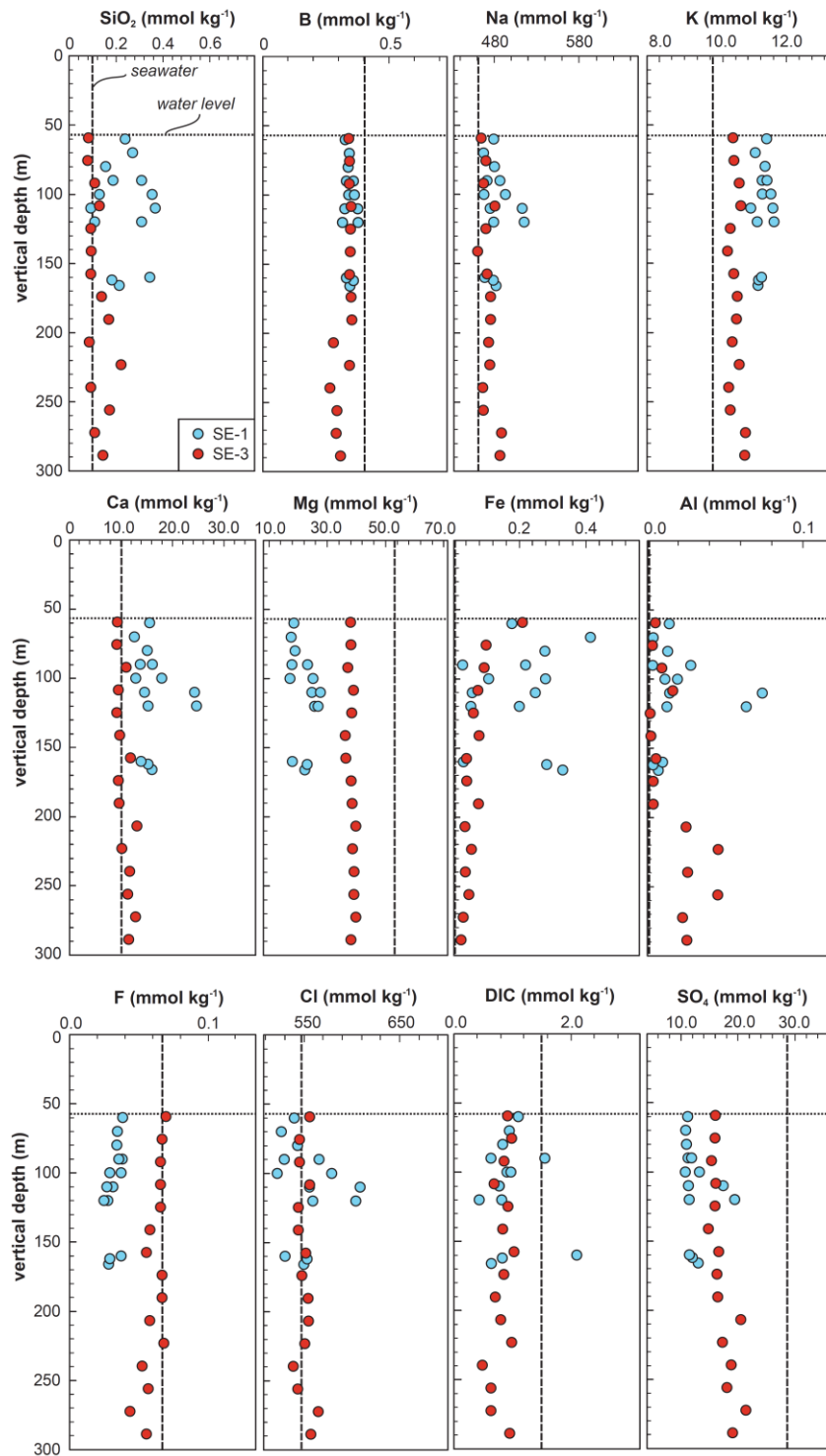
Figure 3. *Elemental concentrations in water samples as a function of vertical depth from SE-1 and SE-3 (Fig. 1c). The horizontal dotted line represents the average water level in the borehole (Jackson et al., 2019b). The vertical dashed line represents the average concentration of the corresponding element in seawater (Bruland, 1983). DIC = dissolved inorganic carbon.*
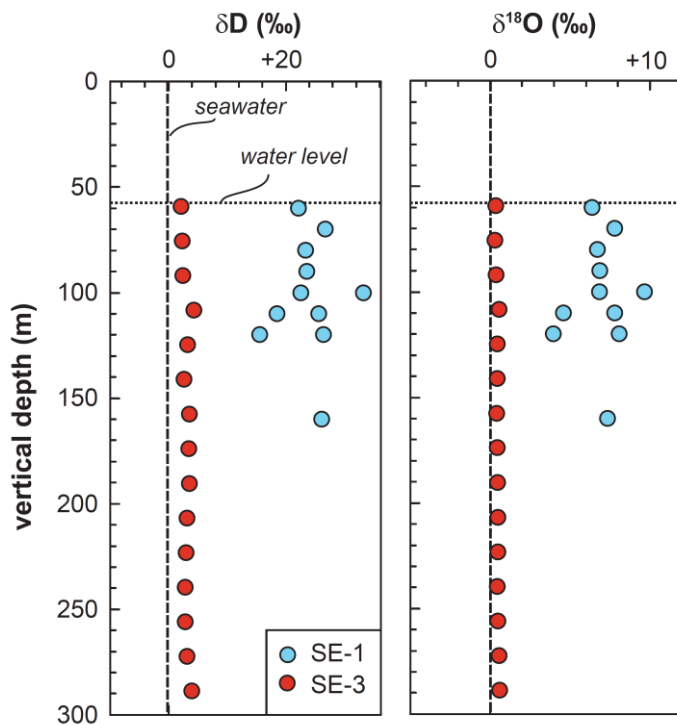
Figure 4. δD and δ¹⁸O measurements as a function of vertical depth in boreholes SE-1 and SE-3. The horizontal dotted line represents the average sea level in the boreholes (Jackson et al., 2019b). The vertical dashed line represents the average concentration of the corresponding element in seawater (Ólafsson and Riley, 1978).

304

305 *Figure 4.* δD and δ¹⁸O measurements as a function of vertical depth in boreholes SE-1 and SE-
306 3. The horizontal dotted line represents the average sea level in the boreholes (Jackson et al.,
307 2019b). The vertical dashed line represents the average concentration of the corresponding
308 element in seawater (Ólafsson and Riley, 1978).

309
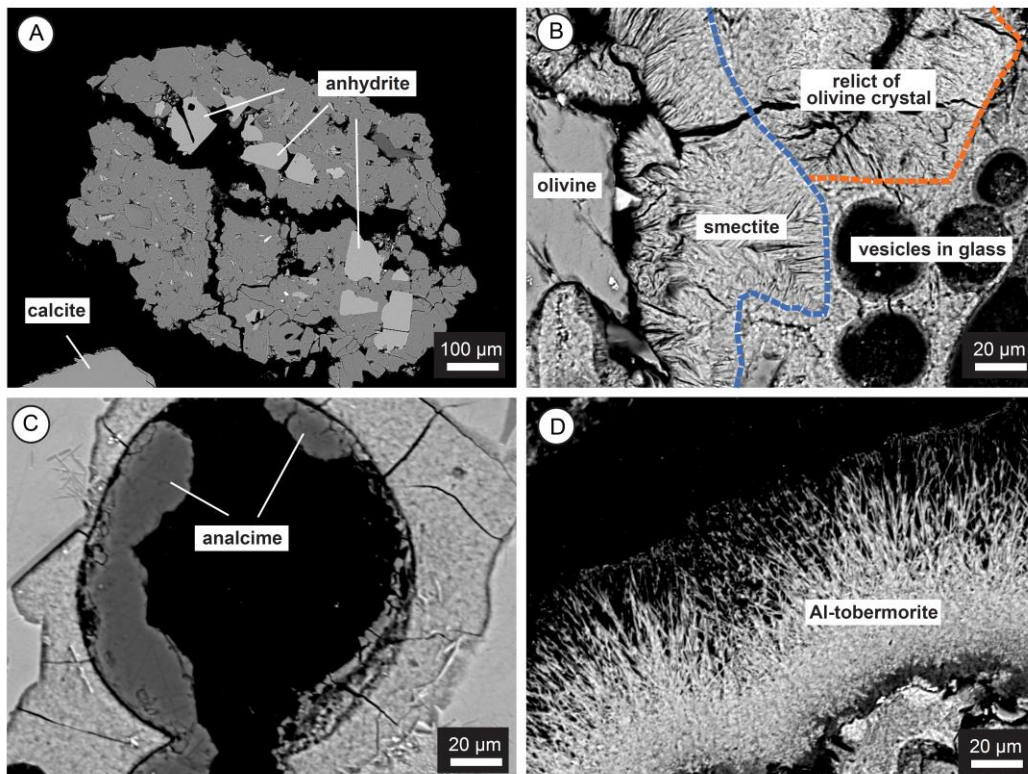
Figure 5. SEM back-scattered electron (BSE) images of the major authigenic minerals identified in the 1979 (Jakobsson and Moore, 1986) and 2017 drill cores. (A) Anhydrite and calcite, ~280 m, SE-03, (B) Alteration rim composed of smectite surrounding olivine, ~90 m, SE-1; dashed lines indicate former outlines of the primary mineral, (C) analcime surface coating in vesicle surrounded by altered glass, ~20 m, SE-1 and (D) Al-tobermorite surface coating in vesicle, ~90 m, SE-1.

4.3. Geochemical modeling

The results of the reaction path simulations between the basaltic glass and seawater are shown in Figure 6. The elemental concentrations of the reacting seawater and the production of authigenic minerals appear to be primarily dependent on the water pH at the modeling temperature, the extent of reaction (i.e, the water-rock ratio), and the redox conditions of the simulated system. At lower temperatures (50-100 °C), the model suggests that the principal authigenic minerals forming at low reaction progress (ξ) are Mg-Fe bearing clay minerals (nontronite, saponite) and zeolites (analcime, chabazite). This suggests limits on the mobility of Si and Al, as well as Mg and Fe. With increasing reaction progress, the model indicates that carbonate minerals (calcite) eventually form, followed by anhydrite and calcium-silicate-hydrates (Al-tobermorite) suggesting limits on the mobility of Ca and SO_4.

At higher temperature, 150 °C, the modelled mineral sequence shows slight differences. The elemental components of anhydrite apparently become supersaturated in the solution. Indeed, anhydrite is among the earliest minerals to form in the model, followed by zeolites and, eventually, carbonates and calcium-silicate-hydrates. Our simulations predict that the precipitation of K-bearing minerals (e.g., Al-tobermorite, K-bearing smectites and zeolites) is limited at low reaction progress. However, with progressive reaction, K will eventually be incorporated into K-bearing mineral phases such as smectitic clay minerals and Al-tobermorite. These findings are in agreement with experimental results by Seyfried Jr and Bischoff (1979) who showed that K concentrations in the solution decreased slightly during basalt alteration at 70 °C. The redox conditions of the system appear to be strongly dependent on the nature and formation of clay minerals that include Fe(III) in their crystalline lattice (e.g., nontronite). The modeling suggests that the abundance of these Fe(III)-bearing mineral phases could control the redox conditions of the thermal system and, thus, the formation of carbonate and sulphate minerals within the simulated temperature range. For example, the formation of calcite and anhydrite, which are carriers of the oxidized species of carbon and sulfur, appears ultimately to be limited at reduced conditions (pe < -6). The precipitation of reduced sulfur-species, such

as pyrite, has less influence on the redox conditions of the system, and only minor amounts (~0.0001-0.01 mol) are calculated to precipitate even at reduced conditions. This is not surprising, as the oxidized sulfur species (SO_4^{2-}) is the dominant species in seawater (Table 2), and anhydrite is the principal mineral phase observed in such low-temperature geothermal environments (Alt, 1995; Alt et al., 1996; Jakobsson and Moore, 1986; Von Damm, 1995). Note, that large amounts of anhydrite in such systems are commonly not observed. The absence of anhydrite from crustal samples has been explained by either retrograde solubility of anhydrite at lower temperature with cooling of the oceanic crust (Alt, 1995; Sleep, 1991) and/or lack of appropriate samples from the oceanic basement (Alt et al., 2003; Teagle et al., 1998).
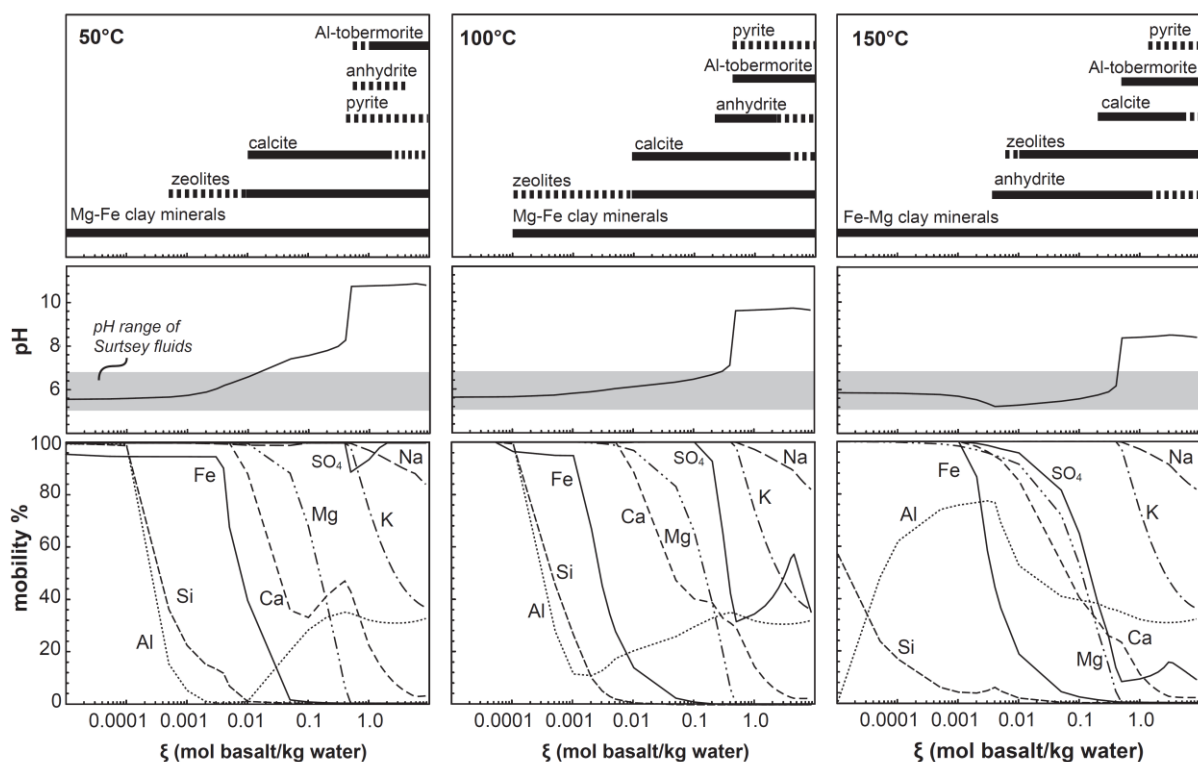
Figure 6. Results from geochemical reaction path modeling using the PHREEQC software (Parkhurst and Appelo, 1999). The simulated authigenic mineralogy, water pH and elemental mobility are shown as a function of reaction progress, ξ, calculated for seawater-basaltic glass interaction at 50, 100 and 150 °C. Mg-Fe clay minerals correspond to nontronite and Mg-Fe-bearing smectites (saponite, nontronite); zeolites correspond to analcime, chabazite and laumontite. These minerals are common in the altered basaltic host rocks at Surtsey and in low-temperature geothermal aquifers within the oceanic crust (this study; Alt et al., 1996; Jakobsson and Moore, 1986; Von Damm, 1995). The abundance of calcite, anhydrite and pyrite mainly depends on the redox conditions of the system. At reduced conditions, pyrite

14

becomes stable whereas the formation of calcite and anhydrite is limited at low water-rock ratios (high reaction progress). Mobility % is a measure of the likelihood of elements remaining in a given solution during water-rock interaction. A high mobility % indicates that consumption of the element by mineral formation is limited, a low mobility % indicates that the element is preferably consumed upon authigenic mineral formation with progressive water-rock interaction.

5. Discussion

5.1. Water origin and effects of evaporation in the boreholes

Both the chemical and the isotopic data of water samples from boreholes SE-1 and SE-3 indicate that seawater is the predominant source of geothermal waters circulating through the submarine Surtsey deposits (Fig. 7; Table 1). Chemical concentrations of Na and Cl of the borehole water samples are generally similar to corresponding seawater concentrations (Fig. 3). Minor deviations from the seawater compositions are observed for B and Ca. Significant departures from the seawater concentrations occur for SiO_2, K, Mg, Fe, Al, SO_4 and DIC in borehole SE-3. These departures can be explained by the processes of water-rock interaction, in which (1) the dissolution of basaltic glass and crystal fragments, principally olivine and labradorite, produces components that are released to the water and/or (2) the crystallization of authigenic mineral assemblages consumes elements from the geothermal water (Fig. 8). The relative enrichment of SiO_2, K, Fe and Al with respect to seawater could possibly also be the result of mixing of cold seawater with a deep-sourced high-temperature geothermal fluid with a chemical composition similar to that measured in the seawater-dominated hydrothermal system at Reykjanes (Arnórsson, 1978). Approximately 5-20% mixing of such a high-temperature geothermal fluid with seawater would be sufficient to explain certain chemical trends observed in the borehole fluids (Fig. A.1). These include increased concentrations of K, Ca and SiO_2 with respect to seawater. The occurrence of clinochlore in the deep submarine SE-1 drill cores could support the existence of alteration induced by a high-temperature fluid (Jackson et al., 2019a). However, the inferred mixing process would also increase CO_2 and H_2S concentrations compared to seawater concentrations; these increases have not been observed in the borehole fluids. Thus, minor input of a deep-sourced high-temperature geothermal fluid could be considered plausible for some concentrations such as K, Ca and SiO_2, but it does not fully explain other compositional variations. Even if a deep-sourced high-temperature fluid is present, it cannot be confirmed with absolute certainty with the borehole water samples because mixing ratios are too low for accurate evaluation.

15

In borehole SE-1, the concentrations of K, Na, Ca and Cl in water samples obtained nearly 40 years after drilling are significantly higher than seawater concentrations or measured concentrations in water samples from borehole SE-3 obtained one year after drilling. The δD and $\delta^{18}O$ values are also significantly more positive than those observed in SE-3 and seawater, as well as reported δD and $\delta^{18}O$ values from the seawater-dominated hydrothermal system at Reykjanes (Ólafsson and Riley, 1978; Sveinbjornsdottir et al., 1986). These differences imply that mixing with a deep-sourced high-temperature fluid does not fully explain the measured chemical trends of the waters in borehole SE-1. Note, in particular, that the steel-cased SE-1 borehole is capped only by a loose lid, and that this covering has been in place for nearly 40 years. By contrast, the 2017 boreholes are capped with well heads that are firmly screwed onto the steel conductor casing (Fig. 2). Furthermore, the measured temperatures in borehole SE-1 (Fig. 1) plot close to the boiling curve of seawater (Fig. 1). We hypothesize that open and closed system evaporation and condensation could contribute to modifications in the SE-1 water geochemistry (Fig. 7).

In general, evaporation leads to the partition of the enriched isotope into the water phase and the depleted isotope into the vapor phase (Horita and Wesolowski, 1994). Evaporation may also cause the enrichment of certain elements (e.g., Cl, Na, K, SiO_2, Ca, SO_4) in the residual water. The effects of these processes on chemical concentrations and isotope values of the geothermal water can be illustrated by simple closed system and Rayleigh (open system) evaporation and distillation (Fig. 7). In SE-3, for example, δD and $\delta^{18}O$ values and $\delta D/Cl$ ratios indicate only limited closed system and/or Rayleigh type evaporation (0-4%). Vapor can escape only from the borehole when the well-head is opened for sampling purposes; this will lead to limited enrichment of Cl and ^2H- and ^{18}O-enriched isotopes in the residual water. By contrast, in SE-1, δD and $\delta^{18}O$ values correspond to Rayleigh type evaporation of up to 90% depending on the evaporation temperature (Fig. 7). The measured δD and $\delta^{18}O$ values are significantly positive suggesting substantial on-going evaporation processes. However, the measured Cl concentrations are significantly lower than expected for such high evaporation rates (Fig. 7). This decoupling of elemental concentration from the isotopic trends also occurs for other mineral forming elements (SiO_2, Na, K, Ca, Mg, Fe, Al, SO_4). Furthermore, the decrease in Cl is accompanied by a decrease in pH (Table 2). Similar trends are commonly observed for the evaporation path of seawater and may be associated with the formation of salts and sulfates (Horita et al., 1993; McCaffrey et al., 1987).

If the cased SE-1 borehole is considered as a partially open system, where vapor or steam has escaped more-or-less continuously through the loosely attached cover, then it is

429 plausible to expect salt precipitation from the residual water as well as dilution by droplets

430 from condensing steam. These processes could produce the decrease in the observed Cl

431 concentrations. However, they would also lead to a simultaneous decrease in δD and $\delta^{18}O$

432 values in the SE-1 waters, which is not the case. Alternatively, the development of authigenic

433 clay minerals upon mineral supersaturation in the borehole water could produce additional ^2H-

434 enrichment in the water, due to the uptake of the ^2H-depleted isotope by incipient clay mineral

435 (Capuano, 1992; Gilg and Sheppard, 1996; Lambert and Epstein, 1980; Lawrence and Taylor,

436 1972; Marumo et al., 1980; Méheut et al., 2007, 2010; Savin and Epstein, 1970; Suzuoki and

437 Epstein, 1976).

438 It seems, therefore, that the water geochemistry of SE-1 reflects a complex interplay

439 between open system evaporation, condensation and associated salt and clay mineral

440 precipitation that has transpired in the cased borehole over the past 40 years. These processes

441 have obscured and modified the original borehole water geochemistry, so that the isotopic and

442 chemical data appear not to be representative of water-rock interaction processes occurring in

443 the basaltic deposits surrounding the borehole. To gain further insights into how changes in the

444 isotopic and elemental composition of the geothermal water in the Surtsey deposits may be

445 influenced by water-rock interaction we turn to geochemical measurements of the waters in

446 borehole SE-3.

447
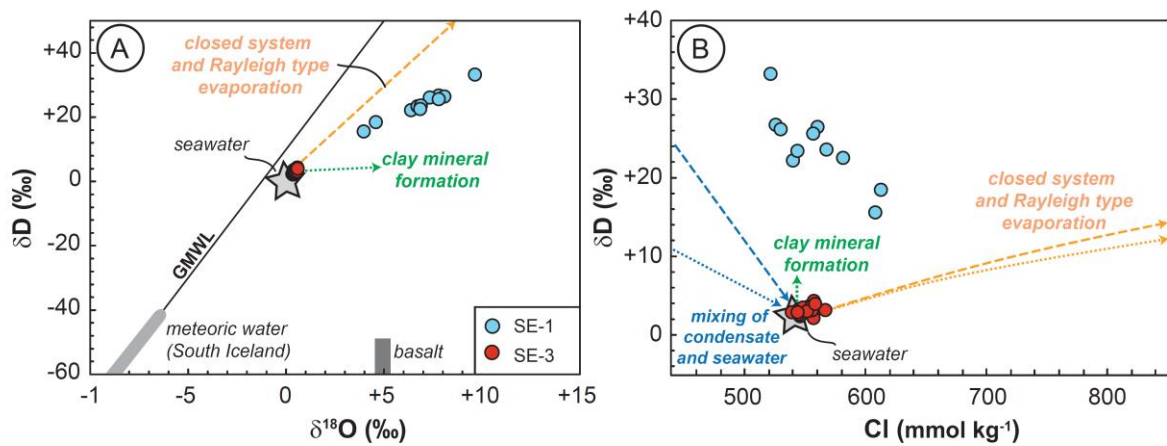
449 *Figure 7. Isotopic variations in water samples from Surtsey boreholes SE-1 and SE-3. (A)*

450 *Comparison with isotopic values typical for seawater (Ólafsson and Riley, 1978), meteoric*

451 *water from the South of Iceland (Stefánsson et al., 2017), and basaltic rocks from Iceland*

452 *(Martin et al., 2017; Nichols et al., 2002). (B) Evolution of Cl concentration and δD values are*

453 *shown for closed system (orange dotted line) and Rayleigh type (orange dashed lines)*

454 *evaporation at 100°C. Closed system and Rayleigh type evaporation of up to 90% may explain*

455 *positive isotopic values in SE-1. However, the Cl concentrations are lower than would be*

456 *expected for such high evaporation rates. SE-1 corresponds to a partially open system with a*

457 *loose-fitting well cover, and a decrease in Cl concentrations may occur through mixing of*

458 *seawater with condensate after Rayleigh type (blue dashed line) or closed system evaporation*

459 *(blue dotted line). Enrichment of ^2H in the geothermal water due to incipient clay mineral*

460 *formation appears to be limited.*

5.2. Elemental mobility and mineral saturation

462 We hypothesize that water-rock interaction in the basaltic lapilli tuff deposits at Surtsey is an

463 incongruent reaction process in which elements are leached, or dissolved, from primary

464 volcanic glasses and crystal fragments; incorporated into interstitial porewater; and then

465 consumed through the formation of authigenic mineral phases – or, conversely, released from

466 the interaction environment in the case of an open chemical system. In the case of closed system

467 environments, these processes can be illustrated by relative elemental mobility. Here, Cl is

468 chosen as a reference element since (1) it is an abundant element in seawater and (2) leaching

469 from the basaltic host rocks as well as uptake by relevant authigenic minerals should be

470 relatively limited due to low concentrations of Cl in both host rock and minerals (Tables 2 and

471 3; Fig. 3). The relationships among SiO_2, B, Na, K, Ca, Mg, Fe, Al, F, DIC and SO_4 to Cl are

472 clarified in Figure 8, along with the corresponding element/Cl ratios for basaltic glass

473 dissolution and seawater (Table 1). SE-1 and SE-3 borehole waters record a substantial increase

474 in SiO_2, K, Ca, Fe, Al and Na elemental concentrations relative to the composition of the

475 seawater that infiltrated the original tephra deposits. The ratios of these elements relative to Cl,

476 are generally higher than the corresponding seawater ratios and follow the corresponding

477 element/Cl ratios of basaltic glass dissolution (Fig. 8).

478 Over the past 50 years, the ongoing crystallization of clay, zeolite and other silicate

479 minerals, as well as carbonate and sulfate minerals has apparently progressively decreased the

480 concentrations of constituent elements (Mg, SO_4, F, B, DIC) in the geothermal fluids within

481 the basaltic deposits (Fig. 8). The observed mineral assemblages in the lapilli tuff deposits are

482 indeed consistent with calculated saturation indices close to saturation (SI ~ 0) for anhydrite,

483 calcite, clays and zeolites (Fig. 9, Table A.2). Note, crystallization of 11 Å Al-tobermorite as

484 well as some Fe-Mg clay minerals may not solely depend on temperature conditions (Coleman

485 et al., 2009; Gherardi et al., 2012; Jantzen et al., 2017). Rather, pH and redox conditions as

486 well as water-rock ratios also influence crystallization processes. For example, in our model,

more alkaline conditions promote the simulated saturation of Al-tobermorite and Mg-Fe-saponite in the reacting water, whereas more acidic and reduced conditions favor the simulated saturation of clay minerals such as nontronite and Fe(III)-bearing smectites (Table A.2). Our geochemical model calculations (Fig. 6) also show the formation of authigenic minerals as a function of changing water-rock ratios, progressive water-rock interaction (i.e., decreasing water-rock ratios), pH and redox conditions. Consequently, element mobility appears to be controlled by both dissolution of basaltic glass and uptake by authigenic minerals that depend, in turn, on a variety of environmental variables such as temperature, pH and redox conditions. The enrichment of SiO_2, K, Ca, Fe, Al and Na in waters from both the SE-1 and SE-3 boreholes relative to seawater implies that the rate of glass dissolution exceeds the uptake of these elements in authigenic minerals. Note, however, chemical trends observed in borehole SE-1 may be also be influenced by diverse in-borehole processes as discussed above.

In contrast, ratios of B, Mg, F, DIC and SO_4 to Cl in the borehole waters are generally lower than the corresponding seawater and rock ratios (Fig. 8). Apart from Mg, these elements occur only in trace concentrations in the host basalt (Tables 1 and 4). These low ratios suggest that there is substantial uptake of these elements in authigenic minerals such as clays, sulfates and carbonates. The elemental uptake by authigenic minerals surpasses the elemental concentrations produced through the dissolution of the host basalt during 50 years of water-rock interaction. The uptake of Mg in clay minerals, for example, must far exceed the Mg concentrations dissolved from basalt. The Mg concentrations measured in the borehole waters are significantly lower than those of seawater suggesting that the seawater that originally infiltrated the tephra deposits (and may continue to infiltrate the deposits in a submarine inflow zone (Jackson et al., 2019b) is a source of Mg for these authigenic minerals.
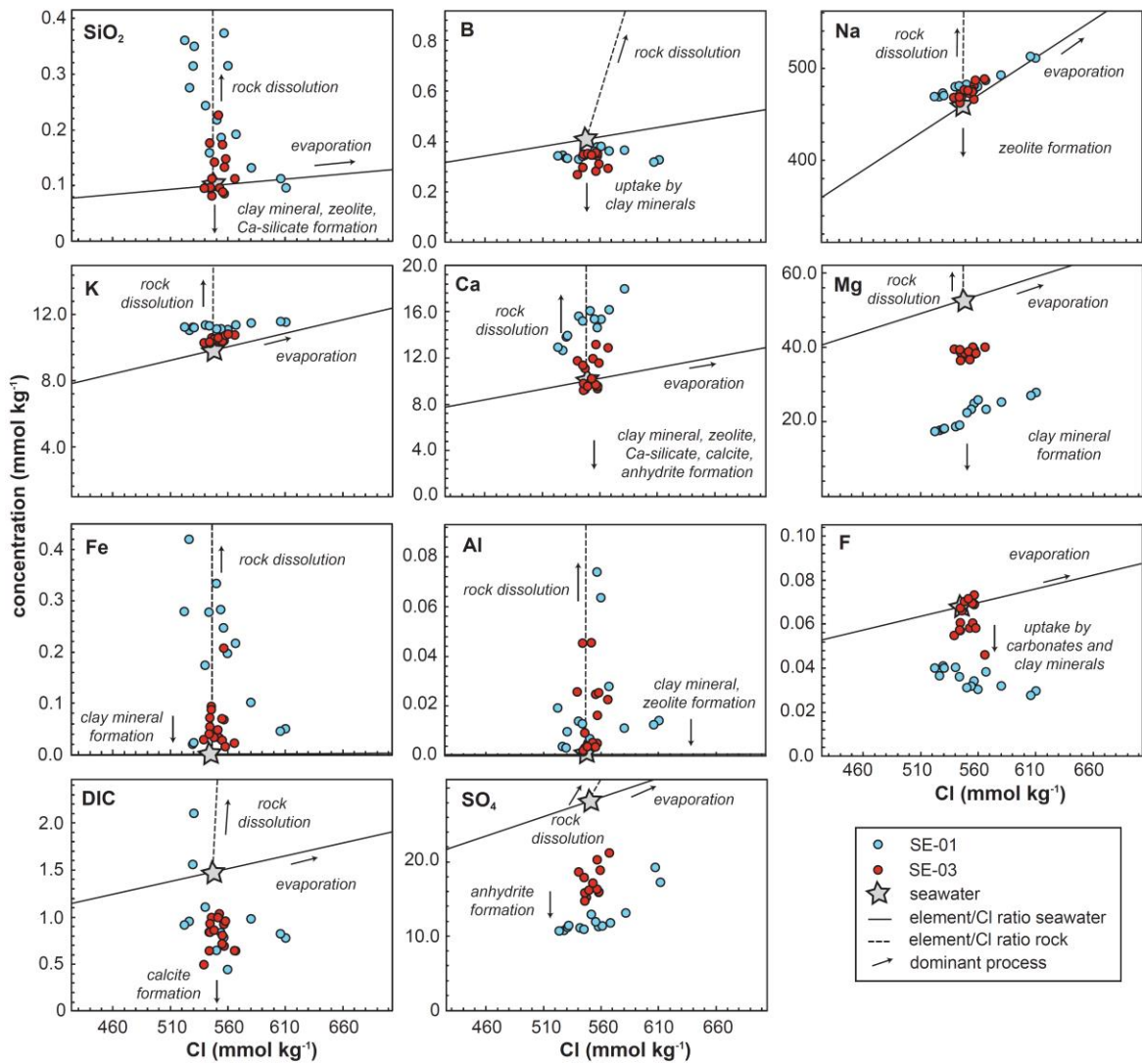
Figure 8. *Elemental mobility relative to Cl concentration in waters sampled from boreholes SE-1 and SE-3. Concentration ratios in SE-1 water samples are different from ratios observed in SE-3 due to complex ongoing open system evaporation and condensation processes in the borehole (Fig. 7). The plots display the predominant processes thought to control the geochemistry of Surtsey borehole waters, through cumulative processes over the 50 years since eruptions terminated. The waters are undersaturated in fluorite. Carbonate and clay minerals may, however, take up F in their crystalline lattice (Carpenter, 1969; Thomas et al., 1977) leading to a decrease in F concentrations in the geothermal water. DIC = dissolved inorganic carbon.*
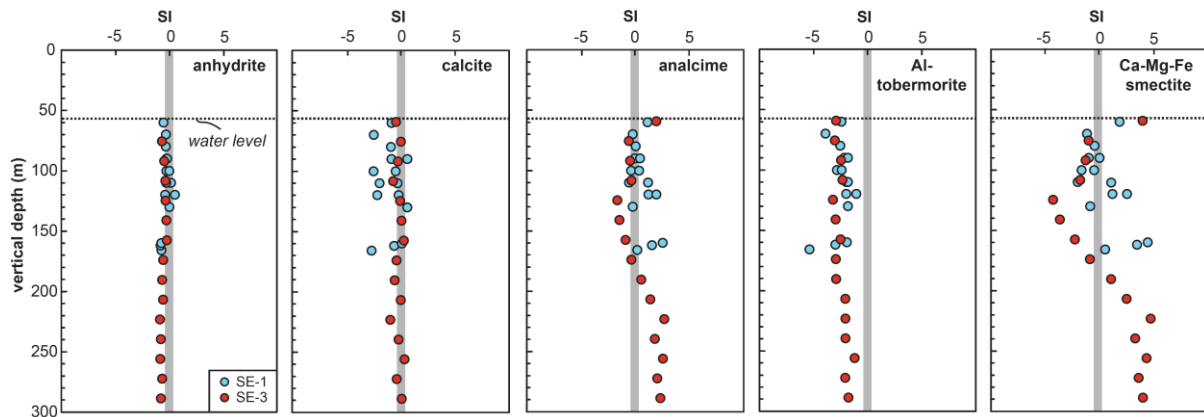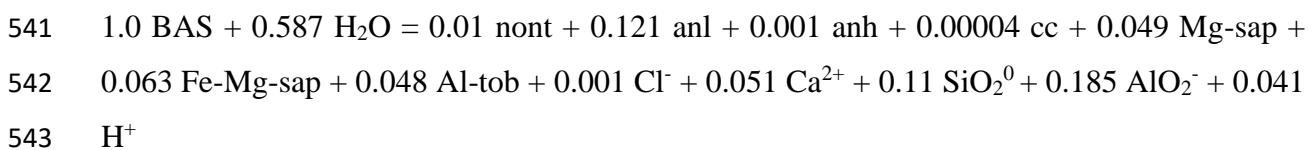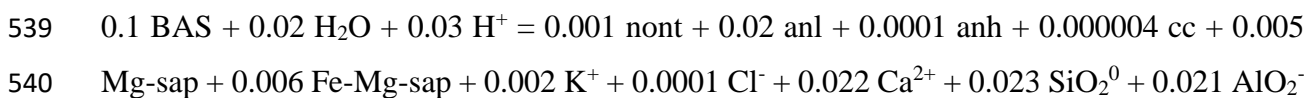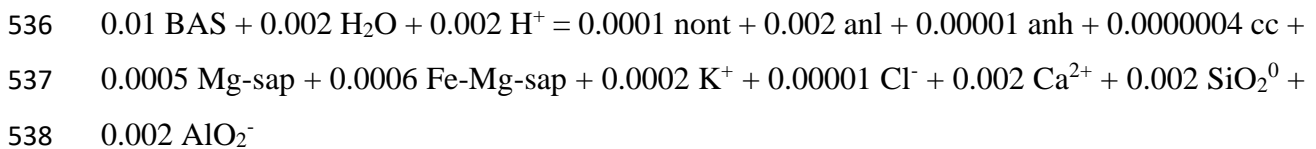
521

522 ***Figure 9***. *Saturation of selected authigenic minerals in borehole waters from Surtsey.*
523 *Saturation indices (SI) were calculated using the PHREEQC software (Parkhurst and Appelo,*
524 *1999). Dissolution reactions and corresponding solubility constants are listed in Table A.2.*
525 *Negative SI values indicate that the water sample is undersaturated in the respective authigenic*
526 *mineral. Positive SI values indicate that the water sample is supersaturated in the respective*
527 *authigenic mineral. The solubility constants for Al-tobermorite were those of Al-tobermorite-*
528 *like cementitious minerals (Table A.2).*

529

530 ### 5.3. Low-temperature (50-150°C) seawater-rock interaction

531 The chemical mass fluxes resulting from basaltic glass dissolution and associated authigenic
532 mineral formation can be clarified using reaction stoichiometry as a function of reaction
533 progress. For a system where approximately 1 g, 10 g and 100 g of basaltic glass interacts with
534 1 kg of seawater the reaction stoichiometry is calculated according to the results of the
535 geochemical modelling at 150 °C (Fig. 6):

536 $0.01\ BAS + 0.002\ H_2O + 0.002\ H^+ = 0.0001\ nont + 0.002\ anl + 0.00001\ anh + 0.0000004\ cc +$
537 $0.0005\ Mg\text{-}sap + 0.0006\ Fe\text{-}Mg\text{-}sap + 0.0002\ K^+ + 0.00001\ Cl^- + 0.002\ Ca^{2+} + 0.002\ SiO_2^0 +$
538 $0.002\ AlO_2^-$

539 $0.1\ BAS + 0.02\ H_2O + 0.03\ H^+ = 0.001\ nont + 0.02\ anl + 0.0001\ anh + 0.000004\ cc + 0.005$
540 $Mg\text{-}sap + 0.006\ Fe\text{-}Mg\text{-}sap + 0.002\ K^+ + 0.0001\ Cl^- + 0.022\ Ca^{2+} + 0.023\ SiO_2^0 + 0.021\ AlO_2^-$

541 $1.0\ BAS + 0.587\ H_2O = 0.01\ nont + 0.121\ anl + 0.001\ anh + 0.00004\ cc + 0.049\ Mg\text{-}sap +$
542 $0.063\ Fe\text{-}Mg\text{-}sap + 0.048\ Al\text{-}tob + 0.001\ Cl^- + 0.051\ Ca^{2+} + 0.11\ SiO_2^0 + 0.185\ AlO_2^- + 0.041$
**543** H^+

The compositions of the basaltic glass and the authigenic minerals are recorded in Tables 2 and 5. Stoichiometries for the same dissolution reactions at 50 and 100°C differ only slightly. The calculated reaction stoichiometries thus indicate that at low reaction progress, that is, high water-rock ratios, the quantities of mineral-forming elements (Ca, SiO_2, Al) leached from the basaltic glass are greater than at low water-rock ratios. Furthermore, the Mg, Fe, SO_4 and CO_2 leached from the glass are predicted to be almost entirely taken up by authigenic clay minerals, carbonates and sulfates even at relatively low reaction progress (Fig. 6). In contrast, the SiO_2, Ca and Al derived from the glass dissolution are predicted to have a somewhat limited uptake into authigenic minerals, even at high reaction progress.

The calculated reaction stoichiometries are, overall, in good agreement with the observed elemental mobility, reaction textures and authigenic mineral assemblages in the geothermal system at Surtsey (Figs. 5 and 8). In addition, K released by basaltic glass dissolution appears to be taken up by the crystallization of K-bearing phillipsite, smectites and Al-tobermorite, which are common authigenic minerals in the 1979 drill core samples (Jackson et al., 2019a; Jakobsson and Moore, 1986; Prause et al., 2020). However, measured K concentrations in the borehole waters are relatively high compared to the corresponding seawater concentration (Figs. 3 and 8). Major element geochemistry of the host basaltic tuff (Jackson et al., 2019b) indicates that as Na_2O increases, K_2O decreases. This may result from early dissolution of glass and precipitation of phillipsite, which then may alter *in situ* to produce analcime (Jackson et al., 2019a; Prause et al., 2020), thus releasing K to the interstitial fluids. The history of K mobility therefore appears complex and depends on interdependent variables involving progressive water-rock interaction, pH and redox conditions that commonly occur in microstructural environments.

Comparing the modelled concentrations of major mineral-forming elements, such as SiO_2, Ca, Mg, SO_4, to the measured concentrations in the water samples from Surtsey borehole SE-3 (Fig. 10) suggests that water-rock interaction and associated basaltic glass dissolution provide a source of SiO_2 and Ca while water-rock interaction and associated authigenic mineral crystallization provides a sink of seawater-derived Mg and SO_4. Note, that questions remain regarding the exact nature of potential water-rock interaction in the cased borehole. The tidal range can be measured in the boreholes (Jackson et al., 2019b) which suggests that the borehole water is presumably not disconnected from the groundwater system of the island. In borehole SE-1, however, complex in-borehole processes may obscure the original geothermal water composition. In contrast, the lack of large variations in the chemical profiles of SE-3 (Fig. 3) suggests that the fluids in this borehole are well mixed. Thus, borehole water in SE-3 may

22

578   potentially represent the geothermal water circulating through the host rocks of Surtsey and,
579   thus, provide an accurate record the impact of low-temperature seawater-basalt interaction on
580   water chemistries.
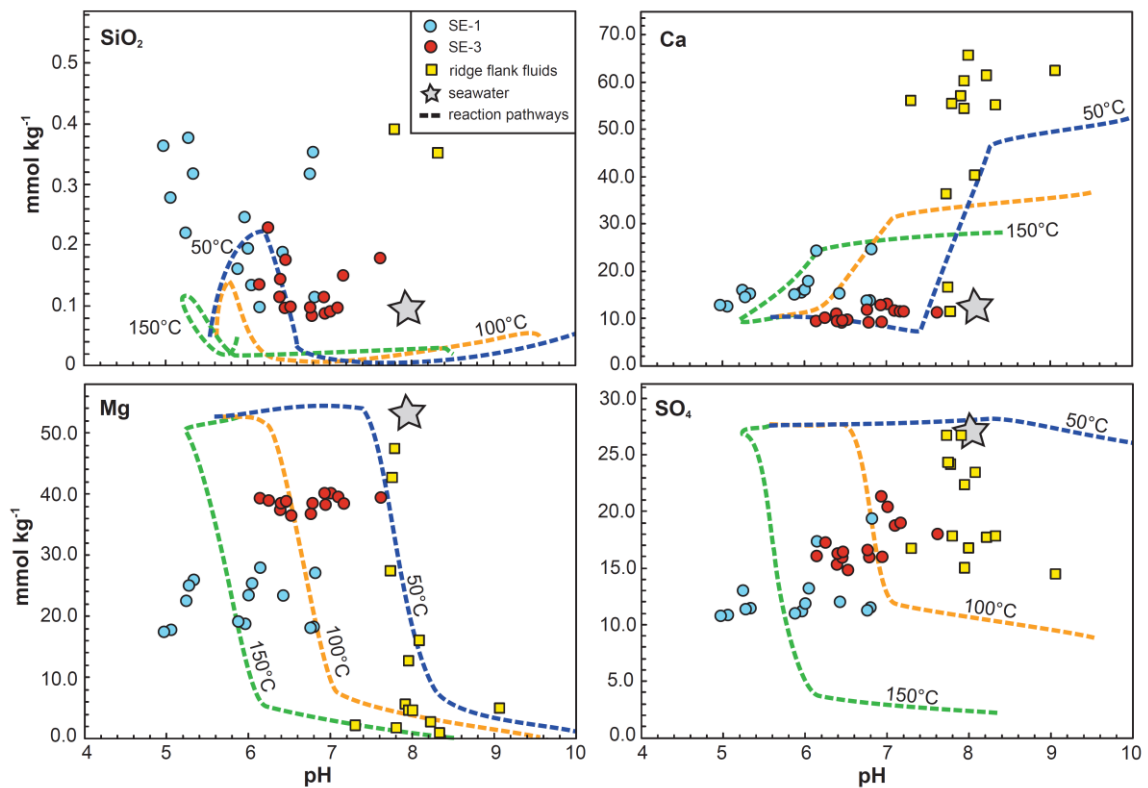
581

582   ***Figure 10.*** *Comparison of measured concentrations in Surtsey borehole waters (this study)*
583   *and ridge flank fluids (Mottl, 1989; Wheat and Fisher, 2008; Wheat and Mottl, 2000) with*
584   *calculated chemical concentrations (dashed lines) at various temperatures and water-rock*
585   *ratios. The pH measured in the borehole water from SE-1 is systematically lower than the pH*
586   *measured in geothermal water collected from SE-3. This may be attributed to complex open*
587   *system evaporation and condensation processes ongoing in SE-1 (Fig. 7).*

588

589   ***5.4. Chemical fluxes in Surtsey in the context of low-temperature aquifers in the oceanic***
590   ***crust***

591   Chemical exchange between circulating seawater and oceanic crust within low-temperature
592   geothermal aquifers produces chemical fluxes with significant effects on oceanic elemental
593   budgets (Alt, 2003; Elderfield and Schultz, 1996; Huang et al., 2018; Mottl and Wheat, 1994;
594   Sansone et al., 1998; Staudigel, 2014; Wheat et al., 1996; Wheat and Mottl, 2000). However,
595   waters from aquifers in low-temperature environments such as ridge flank zones or seamounts
596   are rarely sampled. In addition, their water chemistries are often obscured by sediment-

23

597 seawater interaction processes (Alt, 2003; Coogan and Gillis, 2018; Staudigel, 2014; Wheat
598 and Mottl, 2000).

599   Water circulation in the hydrothermal system at Surtsey is thought to be driven by
600 magmatic intrusions or hot rock at depth (Jakobsson and Moore, 1986). In contrast, water
601 circulation through seamounts in ridge flanks is driven by hydraulic head caused by the
602 difference in density between cold seawater within the recharge zone of one seamount and
603 emission of seawater fluids warmed by cooling of underlying crust and lithosphere in the
604 discharge zone of another seamount (discharge zone) (Fisher and Wheat, 2010; and references
605 therein). The seamounts provide conduits for fluids and form part of the large-scale ridge flank
606 circulation system. Even though the mechanisms of water circulation in Surtsey and ridge flank
607 systems are different, the water chemistries in both settings are controlled primarily by the
608 extent of seawater-basalt reaction and temperature, type and abundance of authigenic minerals.
609 The geothermal water chemistries in the submarine sections of the Surtsey boreholes show
610 similarities to ridge flank aquifers at 10-63 °C in the oceanic crust (Table 4) despite their
611 higher temperature range, up to 141 °C (Jackson et al., 2019b; Jakobsson and Moore, 1986).
612 The Surtsey borehole can thus potentially be viewed as a young and instructive guidepost for
613 the chemical fluxes in the aquifers of ridge flank zones and seamounts. Furthermore, sediment-
614 induced processes are absent at Surtsey, so that investigation of chemical fluxes may be
615 considered solely as the result of hypothesized seawater-basalt interaction.

616   In the following, we extrapolate our geochemical model as well as the dataset from the
617 Surtsey borehole waters to calculate chemical fluxes of these elements between the oceanic
618 crust and seawater (Table 5). Modelled and observed elemental concentrations (Figure 10)
619 provide a framework evaluating the influences of water-basalt alteration processes and
620 temperature on the elemental concentrations measured in geothermal waters from MOR
621 recharge zones but also ridge flank and seamount environments (Table 4). The annual chemical
622 fluxes of SiO_2, Ca, Mg and SO_4 for Surtsey were calculated based on the specific heat flow of
623 the island, water temperatures and the average chemical concentrations measured in borehole
624 SE-3. Details on the calculations and parameters are given in Appendix A.

625   In Surtsey SE-3 borehole waters, SiO_2 and Ca concentrations are enriched with respect
626 to corresponding concentrations in seawater presumably due to the dissolution of basaltic
627 components and the limited uptake of their constituents by authigenic minerals at low-
628 temperature alteration in the range of 44-138 °C. The calculated annual flux of SiO_2 and Ca
629 from the basalt to the seawater ranges from $0.01\text{-}0.03\times10^6$ mol yr^{-1} and $0.3\text{-}1.0\times10^6$ mol yr^{-1},

630 respectively (Table 5). These fluxes are within an order of magnitude (or slightly below) of
631 the estimated SiO_2 and Ca fluxes from the Baby Bare and Dorado seamounts at the eastern
632 flank of the Juan de Fuca Ridge and the eastern flank of the East Pacific Rise, respectively
633 (Mottl et al., 1998; Wheat et al., 2019).

634   The Mg and SO_4 concentrations measured in the Surtsey SE-3 borehole waters are
635 significantly depleted with respect to their corresponding concentrations in seawater. Thus, a
636 significant sink of seawater-derived Mg and SO_4 should occur at the full range of temperatures
637 (44-138 °C) measured in the subsurface deposits. We hypothesize that Mg is consumed during
638 formation of clay minerals, whereas SO_4 is incorporated into anhydrite. The calculated annual
639 fluxes from seawater to the Surtsey basaltic deposits of $6.1\text{-}20\times10^6$ mol yr^{-1} for Mg and 4.8-
640 16×10^6 mol yr^{-1} for SO_4 correspond well with those estimated for Baby Bare and Dorado
641 seamounts (Table 5).

642   These similarities in estimated chemical fluxes as well as heat flow values and water
643 chemistries suggest that the Surtsey geothermal system may deliver insights into low-
644 temperature seafloor alteration processes in MOR recharge zones. Moreover, Surtsey could
645 provide a valuable young analogue for assessing the chemical evolution of fluid discharge over
646 the life cycle of a seamount system.

647

648 *5.5. Implications for global elemental fluxes in the oceanic crust*
649 The simulated elemental concentrations from geochemical modeling at 50-150 °C (Fig. 10,
650 Table A.4) provide a foundation for investigating the dependence of SiO_2, Ca, Mg and SO_4
651 chemical fluxes on temperature and, thus, the associated types and abundance of authigenic
652 mineral formation. The analytical foundation provides insights into water chemistries in
653 aquifers within MOR recharge zones and porewater evolution within the deeper aging oceanic
654 crust where temperatures remain elevated. Flux calculations have been carried out over a
655 temperature range of 50 to 150 °C and for fluid mass fluxes that are characteristic for MOR
656 recharge zones and ridge flank systems, respectively. For details on the flux calculations see
657 Appendix A. Negative flux values indicate the loss of an element from seawater and positive
658 flux values indicate addition of an element to seawater (Table 5).

659   The addition and removal of SiO_2 to and from the ocean through basalt dissolution and
660 authigenic mineral formation, respectively, is found to be rather limited over the 50 to 150 °C
661 temperature range of recharge zones of MORs and ridge flank systems. Yet, estimated chemical
662 fluxes (-0.005 to $+0.1\times10^{12}$ mol yr^{-1}) to the ocean are insignificant compared to the annual

663   riverine SiO_2 influx of $+6.4×10^{12}$ mol yr^{-1} (Mackenzie, 1992). This agrees well with previous

664   findings from global SiO_2 flux estimates for ridge flank and mid-ocean ridge systems that

665   showed that SiO_2 fluxes emitted from these systems are low with respect to the riverine flux

666   (Elderfield and Schultz, 1996; Mottl and Wheat, 1994; Mottl et al., 1998; Sleep, 1991;

667   Staudigel, 2014; Von Damm et al., 1985; Wheat and Fisher, 2008; Wheat and Mottl, 2000).

668   Our model simulations confirm that basalt dissolution at low temperatures in the range

669   of 50-100 °C may induce significant mobility of Ca in water. Calcium dissolution from the

670   altering basalt exceeds the uptake of Ca by Ca-bearing authigenic minerals such as zeolites and

671   silicate hydrates. The annual global Ca flux from the rock to seawater has been calculated to

672   range from $+0.2$ to $+129×10^{12}$ mol yr^{-1}. These flux estimates are in the same range as those

673   calculated previously for ridge flank systems ($+1.5$ to $+230×10^{12}$ mol yr^{-1}) and exceed the flux

674   values of the riverine Ca input to the oceans of $+12×10^{12}$ mol yr^{-1} (Mackenzie, 1992; Mottl,

675   1989; Mottl and Wheat, 1994; Staudigel, 2014; Wheat and Fisher, 2008; Wheat and Mottl,

676   2000). The model simulations suggest however, that with increasing temperature to 150 °C,

677   incorporation of Ca into authigenic minerals becomes increasingly significant. This is reflected

678   in smaller Ca fluxes to ocean waters at elevated temperatures ($+0.2$ to $+1.8×10^{12}$ mol yr^{-1}; Table

679   5). This trend is in agreement with previous findings on low Ca fluxes to seawater from high-

680   temperature hydrothermal mid-ocean ridge systems (Staudigel, 2014; Von Damm et al., 1985).

681   The modelling also confirms that low-temperature basaltic seafloor alteration in the

682   range of 50-150 °C may provide an important sink of seawater-derived Mg. Clay mineral

683   formation may effectively remove up to 100% Mg from seawater. Our model suggests that the

684   uptake of Mg by authigenic minerals is highest at temperatures of 50 °C. This is in agreement

685   with previous findings from the Baby Bare ridge flank and seamount system where water

686   temperatures do not exceed 63 °C and Mg concentrations were extremely low (Mottl and

687   Wheat, 1994; Wheat and Mottl, 2000). There, the Mg flux into the oceanic crust was calculated

688   to be -260 to $+1.0×10^{12}$ mol yr^{-1} (Huang et al., 2018; Mottl, 1989; Staudigel, 2014; Wheat and

689   Mottl, 2000), a range similar to the Mg fluxes (-129 to $-1.3×10^{12}$ mol yr^{-1}) calculated by our

690   model.

691   Water-rock interaction accompanied by the formation of anhydrite at temperatures in

692   the range of 50-150 °C apparently serves as a major sink for seawater-derived SO_4. This would

693   correspond to a SO_4 flux into the oceanic crust of up to $-21×10^{12}$ mol yr^{-1}. These calculated

694   values agree well with the flux range previously calculated for SO_4 fluxes in ridge flank (-50

695   to $-2.0×10^{12}$ mol yr^{-1}) (Wheat and Mottl, 2000) and MOR systems (-1.4 to $+0.8$ mol yr^{-1})

696   (Staudigel, 2014). The higher end of range of values is an order of magnitude larger than

697 calculated riverine SO_4 fluxes to the ocean (3.2×10^{12} mol yr^{-1} (Mackenzie, 1992)) and sulfur

698 fluxes emitted from hydrothermal vents along mid-ocean ridges (0.3-0.8×10^{12} mol yr^{-1}) (Sleep,

699 1991; Von Damm et al., 1985). However, anhydrite may subsequently be dissolved by low-

700 temperature hydrothermal fluids; in this way SO_4 could be regained into the ocean (Alt, 1995).

701   In summary, our flux calculations confirm that low-temperature geothermal aquifers in

702 MOR recharge zones have the potential to influence elemental fluxes to and from the oceanic

703 crust at a global scale. Model-based flux values are generally similar to those estimated for

704 basaltic systems at Surtsey and in ridge flank and seamount systems (Table 5). This implies

705 that our modelling approach is a useful tool for providing insights and estimates on chemical

706 fluxes in shallow geothermal aquifers in the oceanic crust. It also may provide indications for

707 porewater chemistries in the deeper igneous oceanic crust where temperatures are higher and

708 water-rock ratios are lower. Note, however, that in our model seawater reacts with basaltic

709 glass. This is appropriate for Surtsey basalt, which contained a large proportion of fresh glass

710 at the initiation of alteration (Jakobsson and Moore, 1986). Much of the oceanic crust is

711 crystalline, however, except for minor pillow rims and flow margins. The dissolution and

712 reaction rates of the crystalline basalt may be slower than those of basaltic glass (e.g., Seyfried

713 Jr and Janecky, 1985). Even so, flux estimates calculated based on the water chemistries

714 predicted by our modelling approach are similar to those of ridge flank and mid-ocean ridge

715 systems (Alt, 2003; Huang et al., 2018; Mottl and Wheat, 1994; Staudigel, 2014; Wheat and

716 Fisher, 2008; Wheat and Mottl, 2000) implying that the fabric of the basalt may not have a

717 substantial effect on the elemental fluxes.

718

719 **Conclusions**

720 Time-lapse boreholes through the young basaltic deposits of Surtsey volcano create an

721 environment for investigations of the geothermal processes and water-rock interaction that take

722 place during the earliest stages of seawater infiltration into the oceanic crust. Boreholes SE-1,

723 acquired in 1979, and SE-3, acquired in 2017, traverse the submarine geothermal system and

724 SE-3 extends into sub-seafloor basaltic tuff deposits. Borehole water was sampled at

725 approximately 10 m depth intervals in the two cased boreholes to investigate the influence of

726 low-temperature (50-150 °C) water-rock interaction on the chemical compositions of water

727 samples. Elemental concentrations of SiO_2, Na, Ca, and Cl are similar to corresponding

728 seawater concentrations whereas concentrations of B, Mg, F, CO_2 and SO_4 are depleted.

729 Furthermore, the δD and $\delta^{18}O$ values measured in the borehole water are more positive, when

730 compared to the isotopic composition of seawater. Additionally, measured concentrations of

SiO$_2$, K, Ca, Mg, Fe, Al, F and SO$_4$ in borehole SE-1 differ strongly from those measured in SE-3. Geochemical analyses suggest possible evaporation and distillation processes through an open well head over the past 40 years. Chemical and isotopic data demonstrate that borehole water sampled from below sea level resembles geothermal fluids that originated from seawater and reacted with the surrounding basaltic rock, producing authigenic mineral assemblages and a corresponding depletion of certain elements in the water samples. Chemical similarities exist among Surtsey borehole waters, ridge flank and seamount fluids (Mottl, 1989; Mottl and Holland, 1978; Mottl and Wheat, 1994; Wheat and Fisher, 2008; Wheat and Mottl, 2000). Our analyses of the Surtsey borehole waters are therefore used as an analogue to investigate seafloor alteration in low-temperature MOR recharge zones as well as ridge flank zone environments. Coupling measured and calculated concentrations from geochemical modeling constrains elemental fluxes for SiO$_2$, Ca, Mg and SO$_4$ to and from these low-temperature hydrothermal systems in the oceanic crust. The results show that water-rock interaction in the temperature range of 50-150 °C may serve as a significant sink of seawater-derived Mg and SO$_4$, whereas it provides a major source of Ca. This implies that seafloor alteration in low-temperature geothermal systems within the oceanic crust may have large effects on the global elemental budgets of these elements.

References

28

765 Allen, D.E. and Seyfried Jr, W.E. (2003) Compositional controls on vent fluids from
766 ultramafic-hosted hydrothermal systems at mid-ocean ridges: An experimental study at 400°C,
767 500 bars. Geochimica et Cosmochimica Acta 67, 1531-1542.

768 Alt, J.C. (1995) Sulfur isotopic profile through the oceanic crust: Sulfur mobility and seawater-
769 crustal sulfur exchange during hydrothermal alteration. Geology 23, 585-588.

770 Alt, J.C. (2003) Hydrothermal fluxes at mid-ocean ridges and on ridge flanks. Comptes Rendus
771 Geoscience 335, 853-864.

772 Alt, J.C., Davidson, G.J., Teagle, D.A.H. and Karson, J.A. (2003) Isotopic composition of
773 gypsum in the Macquarie Island ophiolite: Implications for the sulfur cycle and the subsurface
774 biosphere in oceanic crust. Geology 31, 549-552.

775 Alt, J.C., Teagle, D.A.H., Laverne, C., Vanko, D.A., Bach, W., Honnorez, J., Becker, K.,
776 Ayadi, M. and Pezard, P.A. (1996) Ridge-flank alteration of upper ocean crust in the eastern
777 Pacific: synthesis of results for volcanic rocks of Holes 504B and 896A, Proceedings - Ocean
778 Drilling Program Scientific Results. National Science Foundation, pp. 435-452.

779 Arnórsson, S. (1978) Major element chemistry of the geothermal sea-water at Reykjanes and
780 Svartsengi, Iceland. Mineralogical Magazine 42, 209-220.

781 Blanc, P., Bourbon, X., Lassin, A. and Gaucher, E.C. (2010) Chemical model for cement-based
782 materials: Temperature dependence of thermodynamic functions for nanocrystalline and
783 crystalline C-S-H phases. Cement and Concrete Research 40, 851-866.

784 Bowers, T.S., Campbell, A.C., Measures, C.I., Spivack, A.J., Khadem, M. and Edmond, J.M.
785 (1988) Chemical controls on the composition of vent fluids at 13°-11° N and 21° N, East
786 Pacific Rise. Journal of Geophysical Research: Solid Earth 93, 4522-4536.

787 Bruland, K.W. (1983) Trace elements in seawater, in: Riley, J.P., Chester, R. (Ed.), Chemical
788 Oceanography. Academic Press Inc. (London) Ltd., London, pp. 157-220.

789 Capuano, R.M. (1992) The temperature dependence of hydrogen isotope fractionation between
790 clay minerals and water: Evidence from a geopressured system. Geochimica et Cosmochimica
791 Acta 56, 2547-2554.

792 Carpenter, R. (1969) Factors controlling the marine geochemistry of fluorine. Geochimica et
793 Cosmochimica Acta 33, 1153-1167.

794 Catalano, J.G. (2013) Thermodynamic and mass balance constraints on iron-bearing
795 phyllosilicate formation and alteration pathways on early Mars. Journal of Geophysical
796 Research: Planets 118, 2124-2136.

797 Coleman, N.J., Trice, C.J. and Nicholson, J.W. (2009) 11 Å tobermorite from cement bypass
798 dust and waste container glass: A feasibility study. International Journal of Mineral Processing
799 93, 73-78.

800 Coogan, L.A. and Gillis, K.M. (2018) Low-temperature alteration of the seafloor: impacts on
801 ocean chemistry. Annual Review of Earth and Planetary Sciences 46, 21-45.

802 Edmond, J.M., Measures, C., McDuff, R., Chan, L., Collier, R., Grant, B., Gordon, L. and
803 Corliss, J. (1979) Ridge crest hydrothermal activity and the balances of the major and minor
804 elements in the ocean: The Galapagos data. Earth and Planetary Science Letters 46, 1-18.

805 Einarsson, P. (2008) Plate boundaries, rifts and transforms in Iceland. Jökull 58, 35-58.

806 Elderfield, H. and Schultz, A. (1996) Mid-ocean ridge hydrothermal fluxes and the chemical
807 composition of the ocean. Annual Review of Earth and Planetary Sciences 24, 191-224.

808 Fisher, A.T. and Wheat, C.G. (2010) Seamounts as conduits for massive fluid, heat, and solute
809 fluxes on ridge flanks. Oceanography 23, 74-87.

810 Friedman, J.D. and Williams, R.S. (1970) Changing patterns of thermal emission from Surtsey,
811 Iceland, between 1966 and 1969.

812 Gale, A., Dalton, C.A., Langmuir, C.H., Su, Y. and Schilling, J.G. (2013) The mean
813 composition of ocean ridge basalts. Geochemistry, Geophysics, Geosystems 14, 489-518.

814 Gherardi, F., Audigane, P. and Gaucher, E.C. (2012) Predicting long-term geochemical
815 alteration of wellbore cement in a generic geological CO_2 confinement site: Tackling a difficult
816 reactive transport modeling challenge. Journal of Hydrology 420, 340-359.

817 Gilg, H.A. and Sheppard, S.M.F. (1996) Hydrogen isotope fractionation between kaolinite and
818 water revisited. Geochimica et Cosmochimica Acta 60, 529-533.

819 Gysi, A.P. and Stefánsson, A. (2011) CO_2-water-basalt interaction. Numerical simulation of
820 low temperature CO_2 sequestration into basalts. Geochimica et Cosmochimica Acta 75, 4728-
821 4751.

822 Hannington, M.D., de Ronde, C.D.J. and Petersen, S. (2005) Sea-floor tectonics and submarine
823 hydrothermal systems. Society of Economic Geologists, pp. 111-141.

824 Hardardóttir, V., Brown, K.L., Fridriksson, T., Hedenquist, J.W., Hannington, M.D. and
825 Thorhallsson, S. (2009) Metals in deep liquid of the Reykjanes geothermal system, southwest
826 Iceland: Implications for the composition of seafloor black smoker fluids. Geology 37, 1103-
827 1106.

828 Hardardóttir, V., Hannington, M. and Hedenquist, J. (2013) Metal concentrations and metal
829 deposition in deep geothermal wells at the Reykjanes high-temperature area, Iceland. Procedia
830 Earth and Planetary Science 7, 338-341.

831 Hasterok, D. (2013) Global patterns and vigor of ventilated hydrothermal circulation through
832 young seafloor. Earth and Planetary Science Letters 380, 12-20.

833 Horita, J., Cole, D.R. and Wesolowski, D.J. (1993) The activity-composition relationship of
834 oxygen and hydrogen isotopes in aqueous salt solutions: II. Vapor-liquid water equilibration
835 of mixed salt solutions from 50 to 100 C and geochemical implications. Geochimica et
836 Cosmochimica Acta 57, 4703-4711.

837 Horita, J. and Wesolowski, D.J. (1994) Liquid-vapor fractionation of oxygen and hydrogen
838 isotopes of water from the freezing to the critical temperature. Geochimica et Cosmochimica
839 Acta 58, 3425-3437.

840 Huang, K.-J., Teng, F.-Z., Plank, T., Staudigel, H., Hu, Y. and Bao, Z.-Y. (2018) Magnesium
841 isotopic composition of altered oceanic crust and the global Mg cycle. Geochimica et
842 Cosmochimica Acta 238, 357-373.

843 Humphris, S.E. and Klein, F. (2018) Progress in deciphering the controls on the geochemistry
844 of fluids in seafloor hydrothermal systems. Annual review of marine science 10, 315-343.

845 Jackson, M.D., Couper, S., Stan, C.V., Ivarsson, M., Czabaj, M.W., Tamura, N., Parkinson,
846 D., Miyagi, L.M. and Moore, J.G. (2019a) Authigenic mineral textures in submarine 1979

847 basalt drill core, Surtsey Volcano, Iceland. Geochemistry, Geophysics, Geosystems 20, 3751-
848 3773.

849 Jackson, M.D., Gudmundsson, M.T., Weisenberger, T.B., Rhodes, J.M., Stefánsson, A.,
850 Kleine, B.I., Lippert, P.C., Marquardt, J.M., Reynolds, H.I., Kück, J., Marteinsson, V.T.,
851 Vannier, P., Bach, W., Barich, A., Bergsten, P., Bryce, J.G., Cappelletti, P., Couper, S.,
852 Fahnestock, M.F., Gorny, C.F., Grimaldi, C., Groh, M., Guðmundsson, Á., Gunnlaugsson,
853 Á.T., Hamlin, C., Högnadóttir, T., Jónasson, K., Jónsson, S.S., Jørgensen, S.L., Klonowski,
854 A.M., Marshall, B., Massey, E., McPhie, J., Moore, J.G., Ólafsson, E.S., Onstad, S.L., Perez,
855 V., Prause, S., Snorrason, S.P., Türke, A., White, J.D.L. and Zimanowski, B. (2019b)
856 SUSTAIN drilling at Surtsey volcano, Iceland, tracks hydrothermal and microbiological
857 interactions in basalt 50 years after eruption. Scientific Drilling 25, 35-46.

858 Jackson, M.D., Moon, J., Gotti, E., Taylor, R., Chae, S.R., Kunz, M., Emwas, A.H., Meral, C.,
859 Guttmann, P. and Levitz, P. (2013) Material and elastic properties of Al-tobermorite in ancient
860 Roman seawater concrete. Journal of the American Ceramic Society 96, 2598-2606.

861 Jackson, M.D., Mulcahy, S.R., Chen, H., Li, Y., Li, Q., Cappelletti, P. and Wenk, H.-R. (2017)
862 Phillipsite and Al-tobermorite mineral cements produced through low-temperature water-rock
863 reactions in Roman marine concrete. American Mineralogist 102, 1435-1450.

864 Jakobsson, S.P. (1978) Environmental factors controlling the palagonitization of the Surtsey
865 tephra, Iceland. Bulletin of the Geological Society of Denmark 27, 91-105.

866 Jakobsson, S.P., Guðmundsson, G. and Moore, J.G. (2000) Geological monitoring of Surtsey,
867 Iceland, 1967-1998. Surtsey Research 11, 99-108.

868 Jakobsson, S.P. and Moore, J.G. (1982) The Surtsey research drilling project of 1979. Surtsey
869 Research 9, 76-93.

870 Jakobsson, S.P. and Moore, J.G. (1986) Hydrothermal minerals and alteration rates at Surtsey
871 volcano, Iceland. Geological Society of America Bulletin 97, 648-659.

872 Jakobsson, S.P., Thors, K., Vésteinsson, Á.T. and Ásbjörnsdóttir, L. (2009) Some aspects of
873 the seafloor morphology at Surtsey volcano: The new multibeam bathymetric survey of 2007.
874 Surtsey Research 12, 9-20.

875 James, R.H., Allen, D.E. and Seyfried Jr, W.E. (2003) An experimental study of alteration of
876 oceanic crust and terrigenous sediments at moderate temperatures (51 to 350 C): Insights as to
877 chemical processes in near-shore ridge-flank hydrothermal systems. Geochimica et
878 Cosmochimica Acta 67, 681-691.

879 Jantzen, C.M., Trivelpiece, C.L., Crawford, C.L., Pareizs, J.M. and Pickett, J.B. (2017)
880 Accelerated Leach Testing of Glass (ALTGLASS): II. Mineralization of hydrogels by leachate
881 strong bases. International Journal of Applied Glass Science 8, 84-96.

882 Johnson, G.K., Flotow, H.E. and O'hare, P.A.G. (1982) Thermodynamic studies of zeolites:
883 analcime and dehydrated analcime. American Mineralogist 67, 736-748.

884 Kadko, D., Baker, E., Alt, J. and Baross, J. (1994) Global impact of submarine hydrothermal
885 processes, RIDGE/VENTS workshop report.

886 Kadko, D., Gronvold, K. and Butterfield, D. (2007) Application of radium isotopes to
887 determine crustal residence times of hydrothermal fluids from two sites on the Reykjanes
888 Peninsula, Iceland. Geochimica et Cosmochimica Acta 71, 6019-6029.

889 Kleine, B.I., Stefánsson, A., Halldórsson, S.A. and Barnes, J.D. (2020) Impact of fluid-rock
890 interaction on water uptake of the Icelandic crust: Implications for the hydration of the oceanic
891 crust and the subducted water flux. Earth and Planetary Science Letters 538, 116210.

892 Kleine, B.I., Stefánsson, A., Halldórsson, S.A., Whitehouse, M.J. and Jónasson, K. (2018)
893 Silicon and oxygen isotopes unravel quartz formation processes in the Icelandic crust.
894 Geochemical Perspectives Letters 7, 5-11.

895 Lambert, S.J. and Epstein, S. (1980) Stable isotope investigations of an active geothermal
896 system in Valles Caldera, Jemez Mountains, New Mexico. Journal of Volcanology and
897 Geothermal Research 8, 111-129.

898 Lawrence, J.R. and Taylor, H.P. (1972) Hydrogen and oxygen isotope systematics in
899 weathering profiles. Geochimica et Cosmochimica Acta 36, 1377-1393.

900 Lothenbach, B., Matschei, T., Möschner, G. and Glasser, F.P. (2008) Thermodynamic
901 modelling of the effect of temperature on the hydration and porosity of Portland cement.
902 Cement and Concrete Research 38, 1-18.

903 Mackenzie, F.T. (1992) Chemical mass balance between rivers and oceans. Encyclopedia of
904 Earth System Science. Academic Press New York 431, 445.

905 Marks, N., Schiffman, P. and Zierenberg, R.A. (2011) High-grade contact metamorphism in
906 the Reykjanes geothermal system: Implications for fluid-rock interactions at mid-oceanic ridge
907 spreading centers. Geochemistry, Geophysics, Geosystems 12.

908 Marks, N., Zierenberg, R.A. and Schiffman, P. (2015) Strontium and oxygen isotopic profiles
909 through 3 km of hydrothermally altered oceanic crust in the Reykjanes Geothermal System,
910 Iceland. Chemical Geology 412, 34-47.

911 Martin, E., Bindeman, I., Balan, E., Palandri, J., Seligman, A. and Villemant, B. (2017)
912 Hydrogen isotope determination by TC/EA technique in application to volcanic glass as a
913 window into secondary hydration. Journal of Volcanology and Geothermal Research 348, 49-
914 61.

915 Marumo, K., Nagasawa, K. and Kuroda, Y. (1980) Mineralogy and hydrogen isotope
916 geochemistry of clay minerals in the Ohnuma geothermal area, northeastern Japan. Earth and
917 Planetary Science Letters 47, 255-262.

918 McCaffrey, M.A., Lazar, B.H.D.H. and Holland, H.D. (1987) The evaporation path of seawater
919 and the coprecipitation of Br (super-) and K (super+) with halite. Journal of Sedimentary
920 Research 57, 928-937.

921 Méheut, M., Lazzeri, M., Balan, E. and Mauri, F. (2007) Equilibrium isotopic fractionation in
922 the kaolinite, quartz, water system: Prediction from first-principles density-functional theory.
923 Geochimica et Cosmochimica Acta 71, 3170-3181.

924 Méheut, M., Lazzeri, M., Balan, E. and Mauri, F. (2010) First-principles calculation of H/D
925 isotopic fractionation between hydrous minerals and water. Geochimica et Cosmochimica Acta
926 74, 3874-3882.

927 Michard, G., Albarede, F., Michard, A.L., Minster, J.-F., Charlou, J.-L. and Tan, N. (1984)
928 Chemistry of solutions from the 13°N East Pacific Rise hydrothermal site. Earth and Planetary
929 Science Letters 67, 297-307.

930 Moore, J.G. (1985) Structure and eruptive mechanisms at Surtsey Volcano, Iceland. Geological
931 Magazine 122, 649-661.

932 Moore, J.G. and Jackson, M.D. (in press) Observation on the structure of Surtsey. Surtsey
933 Research 14, 33-45.

934 Mottl, M.J. (1989) Hydrothermal convection, reaction, and diffusion in sediments on the Costa
935 Rica Rift flank: pore-water evidence from ODP Sites 677 and 678, Becker, K., Sakai, H., et
936 al., Proc. ODP, Sci. Results, pp. 195-213.

937 Mottl, M.J. and Holland, H.D. (1978) Chemical exchange during hydrothermal alteration of
938 basalt by seawater—I. Experimental results for major and minor components of seawater.
939 Geochimica et Cosmochimica Acta 42, 1103-1115.

940 Mottl, M.J. and Wheat, C.G. (1994) Hydrothermal circulation through mid-ocean ridge flanks:
941 Fluxes of heat and magnesium. Geochimica et Cosmochimica Acta 58, 2225-2237.

942 Mottl, M.J., Wheat, G., Baker, E., Becker, N., Davis, E., Feely, R., Grehan, A., Kadko, D.,
943 Lilley, M. and Massoth, G. (1998) Warm springs discovered on 3.5 Ma oceanic crust, eastern
944 flank of the Juan de Fuca Ridge. Geology 26, 51-54.

945 Mottl, M.L. (2003) Partitioning of energy and mass fluxes between mid-ocean ridge axes and
946 flanks at high and low temperature. Energy and mass transfer in marine hydrothermal systems,
947 271-286.

948 Muehlenbachs, K. and Clayton, R.N. (1976) Oxygen isotope composition of the oceanic crust
949 and its bearing on seawater. Journal of Geophysical Research 81, 4365-4369.

950 Neuhoff, P.S. (2000) Thermodynamic properties and parageneses of rock-forming zeolites.
951 Stanford University.

952 Nichols, A.R.L., Carroll, M.R. and Höskuldsson, A. (2002) Is the Iceland hot spot also wet?
953 Evidence from the water contents of undegassed submarine and subglacial pillow basalts. Earth
954 and Planetary Science Letters 202, 77-87.

955 Nielsen, S.G., Rehkämper, M., Teagle, D.A.H., Butterfield, D.A., Alt, J.C. and Halliday, A.N.
956 (2006) Hydrothermal fluid fluxes calculated from the isotopic mass balance of thallium in the
957 ocean crust. Earth and Planetary Science Letters 251, 120-133.

958 Ólafsson, J. and Riley, J.P. (1978) Geochemical studies on the thermal brine from Reykjanes
959 (Iceland). Chemical Geology 21, 219-237.

960 Pálsson, Ó.K., Gislason, A., Guðfinnsson, H.G., Gunnarsson, B., Ólafsdóttir, S.R., Petursdottir,
961 H., Sveinbjörnsson, S., Thorisson, K. and Valdimarsson, H. (2012) Ecosystem structure in the
962 Iceland Sea and recent changes to the capelin (Mallotus villosus) population. ICES Journal of
963 Marine Science 69, 1242-1254.

964 Parkhurst, D.L. and Appelo, C.A.J. (1999) User's guide to PHREEQC (Version 2): A computer
965 program for speciation, batch-reaction, one-dimensional transport, and inverse geochemical
966 calculations. Water-resources investigations report 99, 312.

967 Prause, S., Weisenberger, T.B., Cappelletti, P., Grimaldi, C., Rispoli, C., Jónasson, K., Jackson,
968 M.D. and Gudmundsson, M.T. (2020) Alteration progress within the Surtsey hydrothermal
969 system, SW Iceland–A time-lapse petrographic study of cores drilled in 1979 and 2017. Journal
970 of Volcanology and Geothermal Research 392, 106754.

Sansone, F.J., Mottl, M.J., Olson, E.J., Wheat, C.G. and Lilley, M.D. (1998) CO_2-depleted fluids from mid-ocean ridge-flank hydrothermal springs. Geochimica et Cosmochimica Acta 62, 2247-2252.

Sarkar, A.K., Barnes, M.W. and Roy, D.M. (1982) Longevity of borehole and shaft sealing materials: thermodynamic properties of cements and related phases applied to repository sealing. Pennsylvania State Univ., University Park (USA). Materials Research Lab.

Savin, S.M. and Epstein, S. (1970) The oxygen and hydrogen isotope geochemistry of clay minerals. Geochimica et Cosmochimica Acta 34, 25-42.

Schipper, C.I., Jakobsson, S.P., White, J.D.L., Palin, J.M. and Bush-Marcinowski, T. (2015) The Surtsey magma series. Scientific reports 5, 11498.

Sclater, J.G., Jaupart, C. and Galson, D. (1980) The heat flow through oceanic and continental crust and the heat loss of the Earth. Reviews of Geophysics 18, 269-311.

Seyfried Jr, W.E. and Bischoff, J.L. (1979) Low temperature basalt alteration by sea water: an experimental study at 70°C and 150°C. Geochimica et Cosmochimica Acta 43, 1937-1947.

Seyfried Jr, W.E. and Janecky, D.R. (1985) Heavy metal and sulfur transport during subcritical and supercritical hydrothermal alteration of basalt: Influence of fluid pressure and basalt composition and crystallinity. Geochimica et Cosmochimica Acta 49, 2545-2560.

Sleep, N.H. (1991) Hydrothermal circulation, anhydrite precipitation, and thermal structure at ridge axes. Journal of Geophysical Research: Solid Earth 96, 2375-2387.

Staudigel, H. (2014) Chemical fluxes from hydrothermal alteration of the oceanic crust, in: L, R.R. (Ed.), The Crust. Elsevier, Oxford, pp. 583-606.

Stefánsson, A. (2010) Low-temperature alteration of basalts–the effects of temperature, acids and extent of reaction on mineralization and water chemistry. Jökull 60, 165-184.

Stefánsson, A., Gunnarsson, I. and Giroud, N. (2007) New methods for the direct determination of dissolved inorganic, organic and total carbon in natural waters by Reagent-Free™ Ion Chromatography and inductively coupled plasma atomic emission spectrometry. Analytica chimica acta 582, 69-74.

Stefánsson, A., Hilton, D.R., Sveinbjörnsdóttir, Á.E., Torssander, P., Heinemeier, J., Barnes, J.D., Ono, S., Halldórsson, S.A., Fiebig, J. and Arnórsson, S. (2017) Isotope systematics of Icelandic thermal fluids. Journal of Volcanology and Geothermal Research 337, 146-164.

Stefánsson, V., Axelsson, G., Sigurdsson, O., Guðmundsson, G. and Steingrímsson, B. (1985) Thermal condition of Surtsey. Journal of geodynamics 4, 91-106.

Stein, C.A. and Stein, S. (1994) Constraints on hydrothermal heat flux through the oceanic lithosphere from global heat flow. Journal of Geophysical Research: Solid Earth 99, 3081-3095.

Suzuoki, T. and Epstein, S. (1976) Hydrogen isotope fractionation between OH-bearing minerals and water. Geochimica et Cosmochimica Acta 40, 1229-1240.

Sveinbjornsdottir, A.E., Coleman, M.L. and Yardley, B.W.D. (1986) Origin and history of hydrothermal fluids of the Reykjanes and Krafla geothermal fields, Iceland. Contributions to Mineralogy and Petrology 94, 99-109.

Teagle, D.A.H., Alt, J.C. and Halliday, A.N. (1998) Tracing the chemical evolution of fluids during hydrothermal recharge: Constraints from anhydrite recovered in ODP Hole 504B. Earth and Planetary Science Letters 155, 167-182.

Thomas, J., Glass, H.D., White, W.A. and Trandell, R.M. (1977) Flouride content of clay minerals and argillaceous earth materials. Clays and Clay Minerals 25, 278-284.

Thorarinsson, S., Einarsson, T., Sigvaldason, G. and Elisson, G. (1964) The submarine eruption off the Vestmann Islands 1963-64. Bulletin Volcanologique 27, 435-445.

Thors, K.J. and Jakousson, S.P. (1982) Two seismic reflection profiles from the vicinity of Surtsey, Iceland. Surtsey Research Progress Report 9, 149.

Türke, A., Jackson, M.D., Bach, W., Kahl, W.-A., Gryzbowski, B., Marshall, B., Guðmundsson, M.T. and Jørgensen, S.L. (2019) Design of the Subsurface Observatory at Surtsey Volcano. Scientific Drilling 25, 57-62.

Von Damm, K.L. (1995) Controls on the chemistry and temporal variability of seafloor hydrothermal fluids. Seafloor hydrothermal systems: Physical, chemical, biological, and geological interactions 91, 222-247.

Von Damm, K.L., Edmond, J.M., Grant, B., Measures, C.I., Walden, B. and Weiss, R.F. (1985) Chemistry of submarine hydrothermal solutions at 21°N, East Pacific Rise. Geochimica et Cosmochimica Acta 49, 2197-2220.

Weisenberger, T.B., Gudmundsson, M.T., Jackson, M.D., Gorny, C.F., Türke, A., Kleine, B.I., Marshall, B., Jørgensen, S.L., Marteinsson, V.T., Stefánsson, A., White, J.D.L., Barich, A., Bergsten, P., Bryce, J., Couper, S., Fahnestock, F., Franzson, H., Grimaldi, C., Groh, M., Guðmundsson, Á., Gunnlaugsson, Á.T., Hamlin, C., Högnadóttir, T., Jónasson, K., Jónsson, S.S., Klonowski, A.M., Kück, J., Magnússon, R.L., Massey, E., McPhie, J., Ólafsson, E.S., Onstad, S.L., Prause, S., Perez, V., Rhodes, J.M. and Snorrason, S.P. (2019) Operational Report for the 2017 Surtsey Underwater volcanic System for Thermophiles, Alteration processes and INnovative Concretes (SUSTAIN) drilling project at Surtsey Volcano, Iceland. ICDP Operational Report. GeoForschungsZentrum (GFZ) German Research Centre for Geosciences, 98 pp.

Wheat, C.G., Feely, R.A. and Mottl, M.J. (1996) Phosphate removal by oceanic hydrothermal processes: An update of the phosphorus budget in the oceans. Geochimica et Cosmochimica Acta 60, 3593-3608.

Wheat, C.G. and Fisher, A.T. (2008) Massive, low-temperature hydrothermal flow from a basaltic outcrop on 23 Ma seafloor of the Cocos Plate: Chemical constraints and implications. Geochemistry, Geophysics, Geosystems 9.

Wheat, C.G., Hartwell, A.M., McManus, J., Fisher, A.T., Orcutt, B.N., Schlicht, L.E.M., Niedenzu, S. and Bach, W. (2019) Geology and fluid discharge at Dorado Outcrop, a low temperature ridge-flank hydrothermal system. Geochemistry, Geophysics, Geosystems 20, 487-504.

Wheat, C.G. and Mottl, M.J. (2000) Composition of pore and spring waters from Baby Bare: Global implications of geochemical fluxes from a ridge flank hydrothermal system. Geochimica et Cosmochimica Acta 64, 629-642.

Tables

Table 1. *Chemical composition of geothermal water from Surtsey. F concentrations have been corrected to account for formation of MgF$^+$ complexes (see Appendix A for details).*

sample ID	Date	Depth	t°C	pH		°C	SiO$_2$	B	Na	K	Ca	Mg	Fe	Al	F	Cl	DIC	SO$_4$	δD (H$_2$O)	δ^{18}O (H$_2$O)
		m					mmol kg^{-1}	mmol kg^{-1}	mmol kg^{-1}	mmol kg^{-1}	mmol kg^{-1}	mmol kg^{-1}	mmol kg^{-1}	mmol kg^{-1}	mmol kg^{-1}	mmol kg^{-1}	mmol kg^{-1}	mmol kg^{-1}	‰	‰
Hole SE-1																				
16-SURT-1-1	09/06/2016	70	110	5.07	/	23	0.276	0.347	469	11.0	12.6	17.7	0.418	0.004	0.037	527	0.950	10.9	26.7	7.8
16-SURT-1-2	09/06/2016	90	122	6.83	/	22	0.315	0.336	473	11.2	13.8	18.0	0.021	0.003	0.040	530	1.56	11.3	-	-
16-SURT-1-3	09/06/2016	100	125	5.09	/	22	0.361	0.345	469	11.3	12.9	17.4	0.278	0.019	0.039	522	0.911	10.8	33.2	9.6
16-SURT-1-4	09/06/2016	110	122	5.67	/	22	0.374	0.381	476	10.9	14.6	24.9	0.246	0.074	0.034	557	0.778	11.4	25.6	7.8
16-SURT-1-5	09/06/2016	120	115	5.81	/	22	0.316	0.383	480	11.1	15.3	25.8	0.197	0.063	0.030	560	0.436	11.5	26.4	8.1
16-SURT-1-6	09/06/2016	162	58	6.54	/	23	0.186	0.364	480	11.1	15.3	23.3	0.282	0.003	0.031	554	0.831	12.0	-	-
16-SURT-1-7	09/06/2016	160	60	6.92	/	22	0.351	0.335	470	11.2	13.9	18.1	0.024	0.010	0.039	531	2.10	11.5	26.1	7.3
16-SURT-1-8	09/06/2016	166	54	5.36	/	23	0.218	0.350	483	11.1	16.0	22.4	0.332	0.007	0.031	551	0.640	13.0	-	-
17-SURT-1-1	09/05/2017	60	90	6.11	/	21	0.244	0.332	480	11.4	15.6	18.6	0.174	0.014	0.040	541	1.10	11.2	22.2	6.4
17-SURT-1-2	09/05/2017	80	115	5.98	/	21	0.159	0.343	481	11.3	15.2	19.0	0.277	0.013	0.036	544	0.834	11.0	23.4	6.7
17-SURT-1-3	09/05/2017	90	122	6.18	/	21	0.192	0.365	487	11.4	16.1	23.3	0.217	0.028	0.038	567	0.636	11.9	23.6	6.9
17-SURT-1-4	09/05/2017	100	125	6.11	/	21	0.132	0.368	493	11.5	17.9	25.2	0.102	0.011	0.032	581	0.975	13.2	22.5	6.8
17-SURT-1-5	09/05/2017	110	122	6.27	/	21	0.096	0.329	512	11.6	24.4	27.8	0.051	0.014	0.030	611	0.772	17.3	18.5	4.6
17-SURT-1-6	09/05/2017	120	113	7.06	/	21	0.112	0.321	514	11.6	24.7	26.9	0.046	0.012	0.028	607	0.818	19.4	15.6	4.0

1060 ***Table 1.*** *continued.*

sample ID	Date	Depth	t°C	pH		°C	SiO$_2$	B	Na	K	Ca	Mg	Fe	Al	F	Cl	DIC	SO$_4$	δD (H$_2$O)	δ^{18}O (H$_2$O)
		m					*mmol kg^{-1}*	*mmol kg^{-1}*	*mmol kg^{-1}*	*mmol kg^{-1}*	*mmol kg^{-1}*	*mmol kg^{-1}*	*mmol kg^{-1}*	*mmol kg^{-1}*	*mmol kg^{-1}*	*mmol kg^{-1}*	*mmol kg^{-1}*	*mmol kg^{-1}*	*‰*	*‰*
Hole SE-3																				
18-SURT-3-1	07/20/2018	59	44	7.05	/	21	0.085	0.345	466	10.3	9.3	38.0	0.207	0.005	0.073	557	0.919	16.0	2.1	0.4
18-SURT-3-2	07/20/2018	76	96	6.58	/	21	0.081	0.348	471	10.4	9.2	38.2	0.094	0.003	0.070	546	0.989	16.0	2.4	0.3
18-SURT-3-3	07/20/2018	92	116	6.48	/	21	0.112	0.347	469	10.5	11.1	37.2	0.088	0.009	0.068	546	0.858	15.3	2.4	0.4
18-SURT-3-4	07/20/2018	108	130	6.22	/	21	0.133	0.355	482	10.6	9.5	39.1	0.069	0.016	0.069	557	0.686	16.1	4.3	0.6
18-SURT-3-5	07/20/2018	125	138	6.44	/	21	0.094	0.352	471	10.3	9.2	38.5	0.055	0.002	0.069	545	0.925	15.9	3.2	0.5
18-SURT-3-6	07/20/2018	141	134	6.55	/	21	0.097	0.351	462	10.2	9.8	36.3	0.072	0.002	0.061	545	0.833	14.8	2.6	0.4
18-SURT-3-7	07/20/2018	158	120	6.90	/	21	0.095	0.348	473	10.4	11.9	36.5	0.033	0.005	0.058	553	1.03	16.6	3.6	0.4
18-SURT-3-8	07/20/2018	174	102	6.49	/	21	0.142	0.354	477	10.5	9.5	38.3	0.034	0.004	0.070	549	0.857	16.3	3.5	0.5
18-SURT-3-9	07/20/2018	190	81	6.60	/	21	0.174	0.358	477	10.5	9.6	38.6	0.071	0.004	0.070	556	0.711	16.4	3.6	0.5
18-SURT-3-10	07/20/2018	207	67	7.22	/	21	0.088	0.284	474	10.3	13.1	39.9	0.028	0.025	0.061	556	0.800	20.4	3.1	0.5
18-SURT-3-11	07/20/2018	223	61	6.49	/	21	0.227	0.348	476	10.5	10.2	38.7	0.049	0.045	0.071	552	0.990	17.2	3.0	0.5
18-SURT-3-12	07/20/2018	240	60	7.34	/	21	0.095	0.270	468	10.2	11.7	39.3	0.030	0.026	0.055	540	0.489	18.7	2.9	0.4
18-SURT-3-13	07/20/2018	256	58	8.01	/	21	0.177	0.299	468	10.3	11.3	39.2	0.041	0.045	0.059	544	0.635	18.0	2.9	0.5
18-SURT-3-14	07/20/2018	272	57	7.11	/	21	0.112	0.295	489	10.7	12.8	39.9	0.023	0.023	0.046	567	0.637	21.3	3.1	0.6
18-SURT-3-15	07/20/2018	289	57	7.37	/	21	0.148	0.312	487	10.7	11.5	38.2	0.016	0.025	0.058	558	0.952	19.0	3.9	0.6

1061

1062

1063

1064

1065

1066

1067 ***Table 2.*** *The initial water and rock composition used for geochemical modelling.*

	Seawater[a]	Basalt[b]	
pH	8.2		
Major elements (mmol kg^{-1})		*Major elements (wt.%)*	
SiO_2	0.1	SiO_2	47.1
B	0.411	Al_2O_3	16.6
Na	459	FeO	10.9
K	9.71	Fe_2O_3	1.2
Ca	9.98	MgO	5.3
Mg	52.3	CaO	9.9
Al	0.0004	Na_2O	3.9
Fe	0.0003	K_2O	0.7
CO_2	1.48	S	0.03
Cl	535	H_2O	0.1
SO_4	27.6	*Trace elements (ppm)*	
δD	0±5[c]	CO_2	13
$\delta^{18}O$	0±1[c]	Cl	240
		δD	-80±10[d]
		$\delta^{18}O$	+5±0.2[e]

[a]Bruland (1983)

[b]Jakobsson and Moore (1986)

[c]Ólafsson and Riley (1978)

[d]Martin et al. (2017)

[e]Muehlenbachs and Clayton (1976)

1068

1069

1070

1071

1072

1073

1074

1075

1076

1077

1078

1079

Table 3. *Representative microprobe data of the major authigenic minerals found in the cores*
1081   *from SE-1 and SE-3 at Surtsey.*

	Analcime	smectite	Tobermorite	Anhydrite	Calcite
Negative charge basis	12	22	22	8	6
borehole	SE-1	SE-1	SE-1	SE-3	SE-3
depth (m)	20	90	90	280	280
in wt.%					
SiO_2	52.30	37.19	46.30		
TiO_2		1.01			
Al_2O_3	23.70	9.64	6.98		
FeO	0.09	21.34	0.07		0.02
MnO		0.23	0.01		
MgO	0.03	10.75	0.05		
CaO	1.28	4.34	32.80	41.41	55.78
Na_2O	12.35	0.27	1.59		
K_2O	0.09	0.41	0.48		
$SrO2$				0.13	0.32
BaO				0.020	
SO3				58.04	
CO_2*					43.78
H_2O*	10.15	14.82	11.71		
Total	100.0	100.0	100.0	99.6	99.9
mineral stoichiometry					
Si	1.62	4.51	4.60		
Ti		0.09			
Al(tot)	0.86	1.37	0.82		
Fe(tot)	0.002	2.2	0.01		0.0004
Mn		0.02	0.001		
Mg	0.001	1.94	0.01		
Ca	0.04	0.56	3.49	1.01	0.99
Na	0.7411	0.06	0.31		
K	0.004	0.06	0.06		
Sr				0.002	0.004
Ba				0.0002	
S				0.99	
C					1.00
H	2.10	11.97	7.76		

*calculated stoichiometrically

1083 **Table 4.** *Comparison of average basalt and water composition at Surtsey, ridge flank systems and mid-ocean ridges.*

	Surtsey basalt		MORB[c]	Surtsey water[d]		water from ridge flank systems[e]				water from vents at MOR
	unaltered[a]	altered[b]			spring water (Baby Bare)	pore water (Baby Bare)	pore water (Costa Rica rift flank)	pore water (Dorado seamount)		21°N[f]
				pH	6.9	8.3	7.8			3.4-3.8
				t°C	44-138	25	63	58	10	273-350
Major elements (wt.%)				*Major elements (mmol kg^{-1})*						
SiO_2	47.1	45.9	50.5	SiO_2	0.124	0.360	0.400	-	0.150	15.6-19.5
TiO_2	2.6	2.3	1.7	B	0.331	0.570	0.550	-	0.420	
Al_2O_3	16.6	16.3	14.7	Na	474	473	470	456	462	432-510
FeO	12.1*	-	10.4*	K	10.4	6.88	7.40	7.00	9.80	23.2-25.8
Fe_2O_3	-	13.5**	-	Ca	10.7	55.2	55.5	58.0	10.2	11.7-20.8
MnO	0.3	0.2	0.2	Mg	38.4	0.980	1.80	8.00	52.4	-
MgO	5.3	7.0	7.6	Fe	0.061	-	0.004	-	0.001	0.75-2.42
CaO	9.9	9.0	11.4	Al	0.016	-	-	-	-	0.004-0.005
Na_2O	3.9	4.3	2.8	F	0.064	-	-	-	-	-
K_2O	0.71	0.6	0.2	Cl	551	554	555	546	541	489-579
S	-	0.6	-	DIC	0.821	-	-	-	-	-
H_2O	-	-	-	SO_4	17.2	17.8	17.8	17.0	27	-
loss on ignition		8.7		H_2S	-	-	-	-	-	6.6-8.4

*total iron as FeO

**total iron as Fe_2O_3

[a]Jakobsson and Moore (1986)

[b]Jackson et al. (2019b)

[c]Gale et al. (2013)

[d]this study, average concentrations from SE-3

[e]Mottl (1989); Wheat and Fisher (2008); Wheat and Mottl (2000)

[f]Von Damm et al. (1985)

1084

Table 5. *Local and global chemical fluxes for Surtsey, ridge flank systems, seamounts and mid-ocean ridge systems. Elemental concentrations to calculate the chemical fluxes are taken from Tables 4 and A.4. Negative flux values indicate fluxes from the ocean and positive flux values indicate fluxes to the ocean.*

	Size (km²)	Fluid temperature (°C)	system	heat flow (MW)	fluid mass flux (kg yr⁻¹)	SiO₂	Ca	Mg	SO₄
Local chemical fluxes for Surtsey, Baby Bare and Dorado seamount (given in ×10⁶ mol yr⁻¹)									
Surtsey	0.47	44-138	recharge MOR	7.5	0.4-1.4 ×10⁹	+0.01 to + 0.03	+0.3 to +1.0	-20 to -6.1	-16 to -4.8
Baby Bare seamount[b]	0.5	25-63	ridge flank	2-3	0.4-0.7 ×10⁹	+0.1 to +0.2	+18 to +31	-35 to -20	-4.1 to -7.2
Dorado semaount[c]	0.25	10-30	ridge flank	10-12	3.4-9.9 ×10⁹	+0.2 to +0.5	+0.7 to +2.2	+0.2 to +0.6	-9.4 to -3.2
Global scale chemical fluxes for MOR and ridge flank systems and river influx (given in ×10¹² mol yr⁻¹)									
low-temperature hydrothermal seafloor alteration[d]		50	recharge MOR	1.5-2.1×10⁶	0.2-0.3×10¹⁵	-0.03 to +0.01	+0.2 to +15	-18 to -1.3	-0.1 to +0.05
			ridge flank	7-15×10⁶	1.1-2.5 ×10¹⁵	-0.2 to +0.1	+0.8 to +129	-129 to -6.1	-1.0 to +0.4
		100	recharge MOR	1.5-2.1×10⁶	0.1-0.2×10¹⁵	-0.1 to -0.002	+1.8 to +29	-63 to -3.8	-21 to +0.2
			ridge flank	7-15×10⁶	3.4-9.9 ×10¹⁵	-0.01 to -0.001	+0.4 to +4.1	-8.8 to -0.8	-3.0 to +0.02
		150	recharge MOR	1.5-2.1×10⁶	0.08-0.1×10¹⁵	-0.005 to -0.003	+0.2 to +1.8	-5.9 to -1.3	-2.8 to -0.8
			ridge flank	7-15×10⁶	0.4-0.8 ×10¹⁵	-0.04 to -0.02	+1.2 to +13	-42 to -5.8	-20 to -3.6
Surtsey[e]		44-138	recharge MOR	1.5-2.1×10⁶	0.1-0.4×10¹⁵	+0.006 to +0.03	+0.06 to +0.2	-5.2 to -1.2	-0.9 to -3.9
			ridge flank	7-15×10⁶	0.4-1.2 ×10¹⁵	+0.03 to +0.2	+0.3 to +1.9	-40 to -5.7	-29 to -4.2
ridge flank systems[f]		10-63	ridge flank	7-15×10⁶	0.9-15 ×10¹⁵	-0.1 to +4.0	+1.5 to +230	-260 to +1.0	-50 to -2.0
MOR axis[g]		>150	discharge MOR			+0.3 to +2.4	+0.0054 to +3.1	-2.6 to -1.5	-1.4 to +0.8
river flux[h]						+6.4	+12	+5.4	+3.2

[a]for calculation of heat flow for Surtsey see Appendix A.

[b]physical parameters (size, temperature, heat flow) from Mottl et al. (1998). Chemical fluxes for Baby Bare seamount were based on the specific heat flow and chemical concentration reported in Table 4.

[c] physical parameters (size, temperature, heat flow) from Wheat et al. (2019). Chemical fluxes for Dorado seamount were based on the specific heat flow and chemical concentration reported in Table 4.

[d]calculated from modeled concentrations (Table A.4) using a global heat flux of 1.5-2.1×10¹² Js⁻¹ (Mottl, 2003) and 7-15×1012 Js⁻¹ (Hasterok, 2013; Stein and Stein, 1994) to simulate chemical fluxes in the recharge zone of MOR-related hydrothermal systems and ridge flank systems, respectively.

[e]calculated from measured concentrations (Table 1). Fluxes have been calculated based on a global heat flux of 7-15×10¹² Js⁻¹ (Hasterok, 2013; Stein and Stein, 1994), aquifer temperatures of 44-138°C and assuming a seawater temperature of 2°C at the seafloor Pálsson et al. (2012)

[f]from Huang et al. (2018); Staudigel (2014); Wheat and Mottl (2000) and references therein. Fluxes have been recalculated based on a global heat flux of 7-15×10¹² Js⁻¹ (Hasterok, 2013; Stein and Stein, 1994) and reported aquifer temperatures (Table 4)

[g]from Edmond et al. (1979); Elderfield and Schultz (1996); Mottl and Wheat (1994); Nielsen et al. (2006); Sleep (1991); Staudigel (2014); Von Damm et al. (1985) and references therein
[h]from Mackenzie (1992)